Article

Cell Metabolism

Deubiquitinases Maintain Protein Homeostasis and Survival of Cancer Cells upon Glutathione Depletion

Graphical Abstract

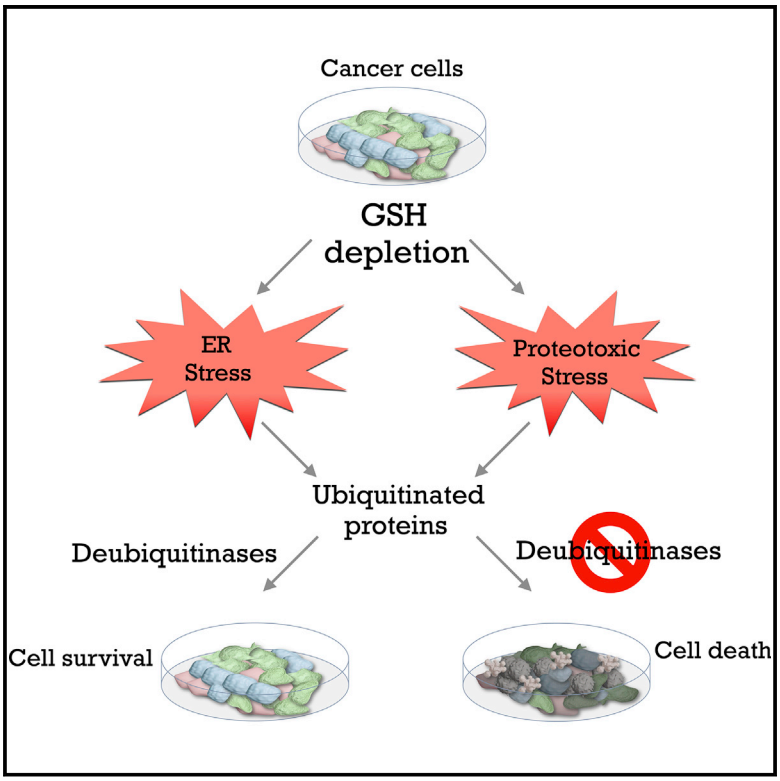

Authors

Isaac S. Harris, Jennifer E. Endress, Jonathan L. Coloff, ..., Gina M. DeNicola, William G. Kaelin, Jr., Joan S. Brugge

Correspondence

joan_brugge@hms.harvard.edu

In Brief

Tumor initiation and progression lead to highly oxidative stress conditions. Harris et al. show that upon glutathione depletion, cancer cells rely on deubiquitinating enzymes to maintain protein homeostasis and cell viability. Combined inhibition of deubiquitinases and glutathione synthesis leads to proteotoxic and ER stress and cell death.

Highlights

- Most cancer cell lines are largely insensitive to GSH depletion
- Deubiquitinases (DUBs) protect cancer cells upon inhibition of GSH synthesis
- Inhibition of DUBs and GSH synthesis causes ER and proteotoxic stress and cell death
- Combined targeting of DUBs and GSH blocks tumor growth

Harris et al., 2019, Cell Metabolism *29*, 1–16
May 7, 2019
https://doi.org/10.1016/j.cmet.2019.01.020

CellPress

Please cite this article in press as: Harris et al., Deubiquitinases Maintain Protein Homeostasis and Survival of Cancer Cells upon Glutathione Depletion, Cell Metabolism (2019), https://doi.org/10.1016/j.cmet.2019.01.020

Cell Metabolism
Article

Deubiquitinases Maintain Protein Homeostasis and Survival of Cancer Cells upon Glutathione Depletion

Isaac S. Harris,[1,2] Jennifer E. Endress,[1,2] Jonathan L. Coloff,[1,2] Laura M. Selfors,[2] Samuel K. McBrayer,[3] Jennifer M. Rosenbluth,[1,2,3] Nobuaki Takahashi,[1,2] Sabin Dhakal,[2] Vidyasagar Koduri,[3] Matthew G. Oser,[3] Nathan J. Schauer,[3] Laura M. Doherty,[3] Andrew L. Hong,[3,4,5] Yun Pyo Kang,[6] Scott T. Younger,[5] John G. Doench,[5] William C. Hahn,[3,5,7] Sara J. Buhrlage,[2,3] Gina M. DeNicola,[6] William G. Kaelin, Jr.,[3] and Joan S. Brugge[1,2,8,*]

[1]Ludwig Cancer Center, Boston, MA 02115, USA
[2]Harvard Medical School, Boston, MA 02115, USA
[3]Dana-Farber Cancer Institute, Boston, MA 02115, USA
[4]Boston Children's Hospital, Boston, MA 02115, USA
[5]Broad Institute of Harvard and MIT, 415 Main Street, Cambridge, MA 02142, USA
[6]Department of Cancer Physiology, Moffitt Cancer Center and Research Institute, Tampa, FL 33612, USA
[7]Brigham and Women's Hospital, Boston, MA 02115, USA
[8]Lead Contact
*Correspondence: joan_brugge@hms.harvard.edu
https://doi.org/10.1016/j.cmet.2019.01.020

SUMMARY

Cells are subjected to oxidative stress during the initiation and progression of tumors, and this imposes selective pressure for cancer cells to adapt mechanisms to tolerate these conditions. Here, we examined the dependency of cancer cells on glutathione (GSH), the most abundant cellular antioxidant. While cancer cell lines displayed a broad range of sensitivities to inhibition of GSH synthesis, the majority were resistant to GSH depletion. To identify cellular pathways required for this resistance, we carried out genetic and pharmacologic screens. Both approaches revealed that inhibition of deubiquitinating enzymes (DUBs) sensitizes cancer cells to GSH depletion. Inhibition of GSH synthesis, in combination with DUB inhibition, led to an accumulation of polyubiquitinated proteins, induction of proteotoxic stress, and cell death. These results indicate that depletion of GSH renders cancer cells dependent on DUB activity to maintain protein homeostasis and cell viability and reveal a potentially exploitable vulnerability for cancer therapy.

INTRODUCTION

Dysregulation of mitochondrial respiration, protein synthesis, and oxygen tension contributes to the increased production of reactive oxygen species (ROS) in cancer cells (Reczek and Chandel, 2015). Oxidative stress, caused by an imbalance between the production of ROS and synthesis of the antioxidant factors that quench them, represents a significant hurdle that impedes tumor initiation and progression (Chio and Tuveson, 2017; Glasauer et al., 2014). Contrary to a longstanding public belief that antioxidants prevent tumor growth, supplementation with antioxidants has been shown to promote tumor incidence and metastasis, not only in mouse models of cancer but also in clinical trials involving dietary antioxidants (Harris and Brugge, 2015; Klein et al., 2011; Le Gal et al., 2015; Piskounova et al., 2015; Sayin et al., 2014).

Glutathione (GSH), a tripeptide formed of cysteine, glutamate, and glycine, is the most abundant antioxidant in the cell (Winterbourn and Hampton, 2008). The rate-limiting step in GSH synthesis is the condensation of glutamate and cysteine by the glutamate-cysteine ligase (GCL) holoenzyme (Meister and Anderson, 1983). GCL comprises a catalytic subunit (GCLC) and a modifying subunit (GCLM), which lacks catalytic activity but promotes GSH synthesis by decreasing the Km for glutamate and increasing the Ki for GSH (Huang et al., 1993). Importantly, evidence suggests that this rate-limiting step is non-redundant (Shi et al., 2000), with GSH synthesis being governed solely by this holoenzyme. Oncogenic mutations have been shown to increase transcription of *GCLC* (DeNicola et al., 2011), and levels of GSH and its rate-limiting metabolite cysteine have been shown to increase with tumor progression in patients (Hakimi et al., 2016). Furthermore, both primary and metastasized tumors have been shown to utilize the reducing factor nicotinamide adenine dinucleotide phosphate, reduced (NADPH) to regenerate GSH stores and survive oxidative stress (Jiang et al., 2016; Piskounova et al., 2015).

Blocking antioxidant production, including the synthesis of GSH, has long been viewed as a potential mechanism to treat cancers (Arrick et al., 1982; Hirono, 1961). Treatment of patients with l-buthionine-sulfoximine (BSO) (Griffith and Meister, 1979), an inhibitor of GCLC, is well tolerated and has been used in combination with the alkylating agent melphalan in multiple phase 1 clinical trials with mixed results (NCT00005835 and NCT00002730) (Bailey, 1998; Villablanca et al., 2016). Inhibition of GSH synthesis has been shown to prevent tumor initiation in multiple mouse models of spontaneous tumorigenesis; however, limited effects have been reported in established

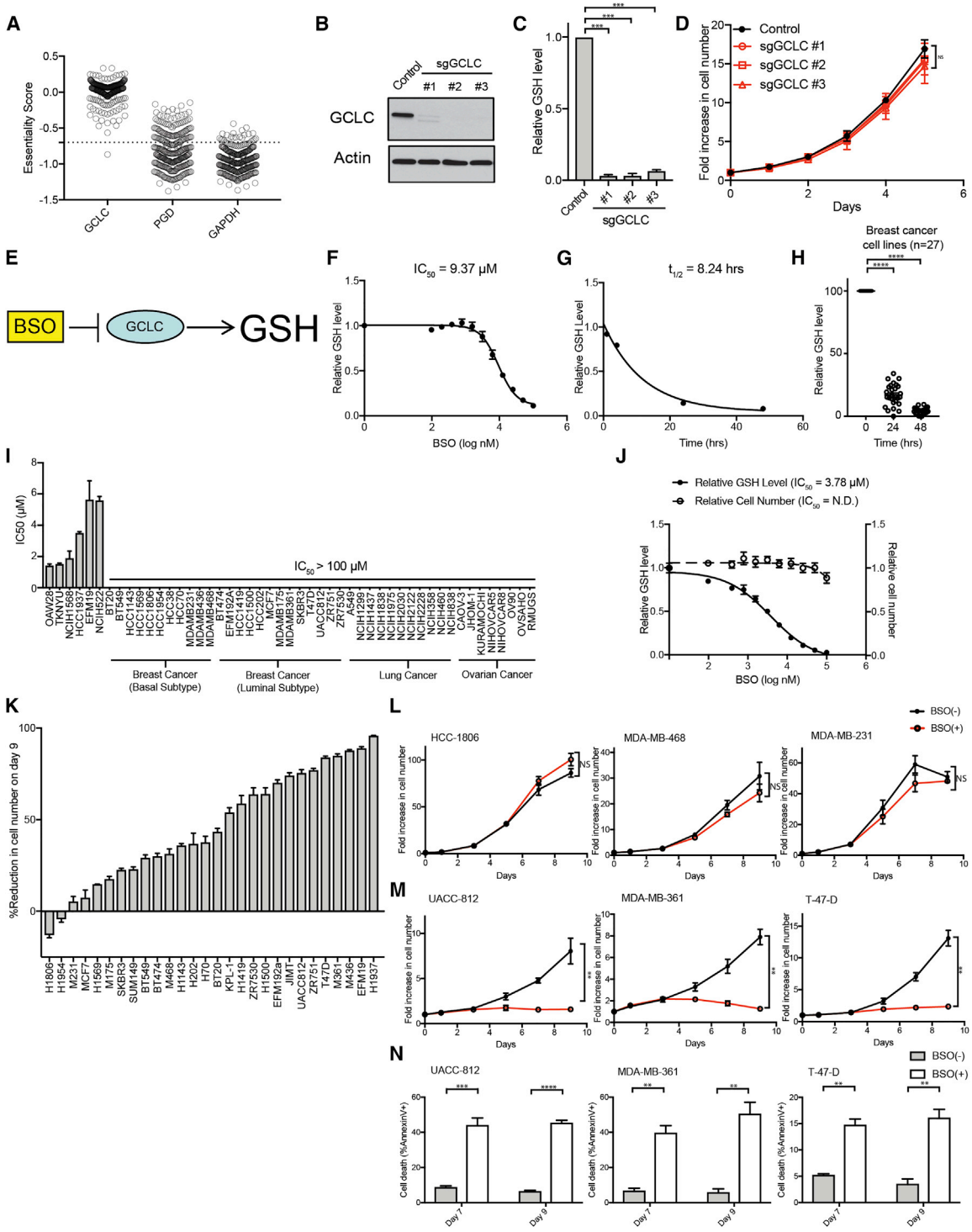

Figure 1. A Subset of Cell Lines Display Sensitivity to Inhibition of GSH Synthesis

(A) Essentiality scores for *GCLC*, *PGD*, and *GAPDH* from pooled CRISPR screens in 340 cancer cell lines conducted during the Achilles project (dotted line refers to a score of −0.6, a cutoff for cellular essentiality).

(B) Representative immunoblot analysis of GCLC protein from HCC-1806 breast cancer cells transduced with LentiCrisprV2 with control sgRNA or sgRNA targeting *GCLC*.

(C and D) (C) Relative GSH levels and (D) fold increase in cell numbers from day 1 from control and sgGCLC HCC-1806 breast cancer cells. Data shown as mean ± SEM from two independent experiments.

(E) Schematic of BSO inhibiting GCLC and blocking GSH synthesis.

(legend continued on next page)

tumors (Harris et al., 2015). Another major antioxidant pathway, governed by the protein thioredoxin 1 (TXN), has been shown to support survival of cells upon GSH depletion. Treatment of thioredoxin-reductase-1 (*Txnrd1*)-null mouse embryonic fibroblasts (MEFs) with BSO or the combined delivery of BSO and auranofin, an inhibitor of TXNRD1, to cancer cells induces potent cytotoxicity (Eriksson et al., 2009; Harris et al., 2015; Mandal et al., 2010; Prigge et al., 2017; Stafford et al., 2018).

A systematic analysis of the role of GSH in cancer cells that have adapted to oxidative stress during tumorigenesis has yet to be reported. In the present study, we carried out such an analysis and show that most cancer cell lines are largely unaffected by GSH depletion. A subset of cancer cell lines is sensitive to inhibition of GCLC, and this sensitivity is only manifested with continuous treatment over the course of several days. To understand the factors underlying this resistance, we carried out genetic and pharmacologic screens of cancer cells under conditions of GCLC inhibition. We found that cells become sensitive to depletion of GSH when enzymes responsible for deubiquitination are inhibited. Combined suppression of GCLC and deubiquitinating enzymes (DUBs) leads to a high level of proteotoxic stress and results in cell death, suggesting that DUB activity is critical to maintain homeostasis in the context of GSH depletion.

RESULTS

Only a Subset of Cancer Cell Lines Is Dependent on GSH Synthesis

To assess the contribution of GSH synthesis to cell survival, we examined publicly available data from genome-scale pooled CRISPR-Cas9 screens conducted across more than 300 cancer cell lines (Doench et al., 2016; Meyers et al., 2017). Loss of *GCLC* caused minimal effects on proliferation across cancer cell lines, as indicated by a *GCLC* essentiality score close to zero (Figure 1A). This score contrasted with those from other non-redundant metabolic genes such as those encoding phosphogluconate dehydrogenase (*PGD*), a component of the oxidative pentose phosphate pathway, and the glycolytic enzyme glyceraldehyde 3-phosphate dehydrogenase (*GAPDH*), both of which had essentiality scores below the −0.6 threshold for the majority of cancer cell lines tested, indicating their requirement for survival (Figure 1A) (Meyers et al., 2017). To further evaluate GCLC dependency, we deleted *GCLC* in the human breast cancer cell line HCC-1806 (a cell line with an essentiality score for *GCLC* above the −0.6 threshold) (Figure 1B). Deletion of *GCLC* caused a drastic reduction in GSH levels without any effect on cellular proliferation (Figures 1C and 1D), mirroring the results observed in the published pooled CRISPR screens. To evaluate the differential sensitivity of cancer cell lines to GSH depletion more quantitatively, we used an inhibitor of GCLC, BSO (Griffith and Meister, 1979), to evaluate the effects of titratable depletion of GSH across a large panel of cancer cell lines (Figure 1E). The efficacy of BSO was confirmed by assessment of the reduction in GSH levels; BSO induced potent and rapid depletion of GSH within 48 h (Figures 1F, 1G, and S1A). Extending this analysis to a larger panel of breast cancer cell lines revealed near uniform kinetics of GSH depletion by BSO (Figure 1H). The effect of BSO on cell number after 72 h was determined for 49 cell lines derived from breast cancer (both basal and luminal subtypes), lung cancer, and ovarian cancer. Across all tumor types, the majority of cancer cell lines displayed no reduction in cell number after depletion of GSH by BSO (Figures 1I, 1J, and S1B–S1E). Interestingly, a minority of cell lines (six) was highly sensitive to BSO, with IC_{50} values ranging from 1 to 6 μM (matching the IC_{50} values for depletion of intracellular GSH). To identify candidate genes underlying sensitivity to GSH depletion, RNA sequencing (RNA-seq) data obtained from the Cancer Cell Line Encyclopedia (CCLE) were analyzed (Barretina et al., 2012; Cancer Cell Line Encyclopedia Consortium and Genomics of Drug Sensitivity in Cancer Consortium, 2015). Fewer than 30 genes were differentially expressed in the six highly sensitive cell lines relative to the other cancer cell lines (Table S1). These genes were not investigated further because the cell lines were derived from diverse tissues, and it was not feasible to determine whether the observed expression differences were actually due to dominant expression patterns driven by the tissue of origin (Hoadley et al., 2018; Selfors et al., 2017).

Since only a minority of cancer cell lines were sensitive to BSO treatment for 72 h (a time point where GSH levels were maximally depleted, as well as a typical time frame to assess drug sensitivity) (Garnett et al., 2012), the response of cancer cells to longer-term depletion of GSH was examined in a large panel of breast cancer cell lines cultured continuously in a single dose of BSO (100 μM) for 9 days. Interestingly, while many cancer cell

(F and G) Relative GSH levels in HCC-1806 breast cancer cells treated with (F) BSO at indicated concentrations for 72 h and (G) BSO at 100 μM for indicated time points. Data shown as mean ± SEM from three independent experiments.

(H) Relative GSH levels in breast cancer cell lines treated with BSO at 100 μM for indicated time points. Data shown as mean ± SEM for 27 breast cancer cell lines.

(I) IC_{50} values for basal (n = 12) and luminal (n = 14) breast cancer cell lines, lung cancer cell lines (n = 13), and ovarian cancer cell lines (n = 10) treated with BSO for 72 h. Data shown as mean ± SD from four technical replicates.

(J) Relative GSH levels and relative cell numbers for MDA-MB-468 breast cancer cells treated with BSO at indicated concentrations for 72 h. Data shown as mean ± SD from four technical replicates.

(K) Percent reduction in cell numbers on day 9 ($[BSO(-)_{Cell\ Number} - BSO(+)_{Cell\ Number}]/BSO(-)_{Cell\ Number}) * 100\%$) for basal (n = 13) and luminal (n = 15) breast cancer cell lines cultured with vehicle or BSO (100 μM) (media with vehicle and BSO replenished every 48 h). Data shown as mean ± SD from three technical replicates and representative of two independent experiments.

(L and M) Fold increase in cell numbers from day 0 of (L) resistant and (M) sensitive breast cancer cell lines treated as in (K) for 9 days. Data shown as mean ± SEM from three independent experiments.

(N) Percentage of cell death determined by Annexin V+ staining in sensitive breast cancer cells treated as in (K) for 9 days. Data shown as mean ± SEM from three independent experiments. NS, not statistically significant; $^{**}p < 0.01$, $^{***}p < 0.001$, $^{****}p < 0.0001$.

Dunnett's multiple comparisons test was used to determine statistical significance for (C) and (H). Two-way ANOVA was used to determine statistical significance for (D), (L), and (M). Unpaired two-tailed t test was used to determined statistical significance for (N). See also Figure S1 and Table S1.

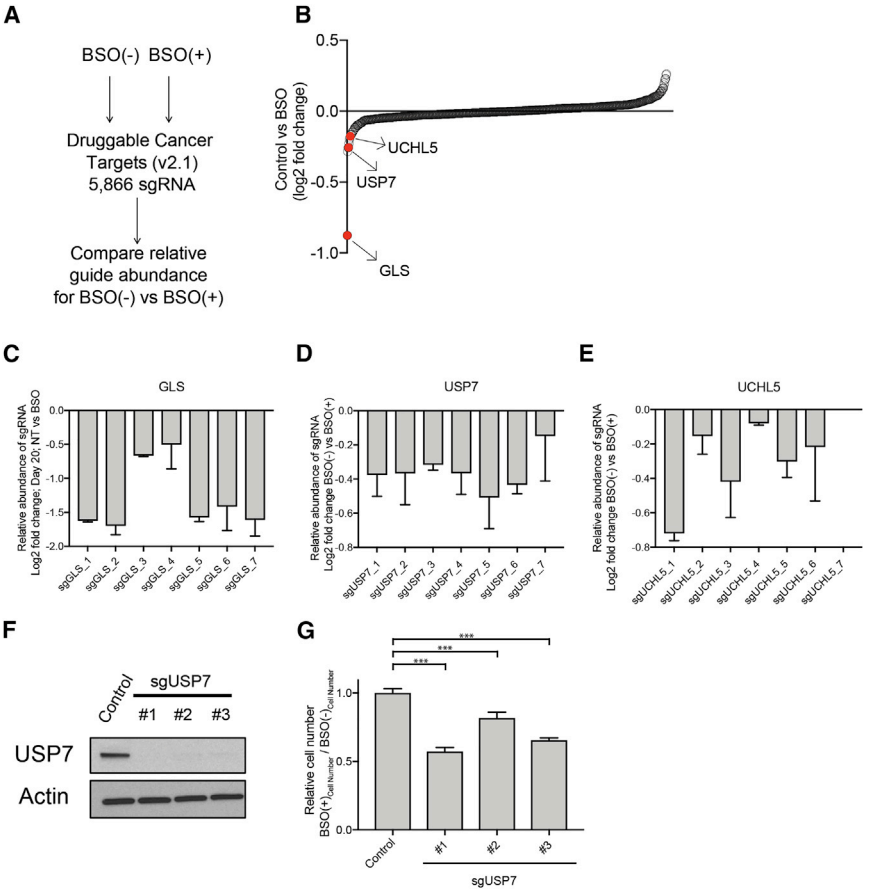

Figure 2. Genetic Screening Reveals Proteins Supporting Survival of Cancer Cells upon GSH Depletion

(A) Schematic of genetic screening of HCC-1806 breast cancer cells with pooled CRISPR library against "druggable" genes treated with vehicle or BSO (500 μM).

(B–E) Relative sgRNA guide abundance for (B) the entire library and individual sgRNAs against (C) *GLS*, (D) *USP7*, and (E) *UCHL5* for HCC-1806 breast cancer cells treated with vehicle or BSO (500 μM) for 16 days. Data shown as mean ± SD from two technical replicates.

(F) Representative immunoblot analysis of USP7 protein from HCC-1806 breast cancer cells transduced with LentiCrisprV2 with control sgRNA or sgRNA targeting *USP7*.

(G) Relative cell numbers (normalized to untreated cells) for control or sgUSP7 HCC-1806 breast cancer cells treated with vehicle or BSO (100 μM) for 14 days. Data shown as mean ± SD from three technical replicates and representative of two independent experiments. ***$p < 0.001$. Dunnett's multiple comparisons test was used to determined statistical significance for (G). See also Tables S2 and S3.

lines were unaffected, we detected a gradient of sensitivities, with a number of lines being sensitive to this longer-term treatment with BSO (Figures 1K–1M, S1F, and S1G). Furthermore, BSO was cytotoxic rather than cytostatic in the sensitive lines as demonstrated by the high percentage of cell death (Figure 1N).

Both TXNRD1 and glutathione peroxidase 4 (GPX4) play critical roles in regulating the sensitivity to oxidative stress and depletion of GSH (Eriksson et al., 2009; Harris et al., 2015; Mandal et al., 2010; Prigge et al., 2017; Stafford et al., 2018; Yang et al., 2014). To assess whether differential expression of these proteins is associated with the observed responsiveness of cancer cells to BSO, TXNRD1 activity and protein expression, as well as GPX4 protein expression, were measured in two BSO-sensitive (T-47D and MDA-MB-361) and two BSO-resistant (HCC-1806 and MDA-MB-468) breast cancer cell lines (Figures S1H–S1J). There were no significant differences in TXNRD1 activity in the four cell lines, and minor differences in the levels of either protein were not consistent with differences in sensitivity to BSO, suggesting that neither differential activity nor expression of either TXNRD1 or GPX4 governs sensitivity to GSH depletion in these breast cancer cell lines.

Overall, these results indicate that cancer cell lines display differential sensitivity to inhibition of GSH synthesis and define both highly sensitive and resistant groups. Furthermore, these findings demonstrate that an extended time under conditions of GSH depletion is required to manifest a cytotoxic phenotype in sensitive cancer cells.

Genetic and Pharmacologic Screening Reveals Factors Promoting Resistance to GCLC Inhibition

To better understand the factors supporting survival of cancer cells upon depletion of GSH, we undertook a genetic screening approach in the highly resistant cancer cell line HCC-1806. We utilized a CRISPR-Cas9 single guide RNA (sgRNA) library that targets more than 750 genes encoding druggable proteins (Druggable Cancer Targets v2.1; Table S2) (Hong et al., 2016) and identified sgRNAs that were differentially depleted or enriched in cancer cells continuously treated with a high dose of BSO (500 μM) (Figures 2A and 2B; Table S3). Under conditions of GCLC inhibition by BSO, a small number of genes scored as significant dropout hits in the CRISPR-Cas9 screen, including glutaminase (*GLS*) and the DUBs ubiquitin-specific protease 7 (*USP7*) and ubiquitin C-terminal hydrolase L5 (UCHL5) (Figures 2B–2E). Inhibition of GLS activity was previously shown to synergize with BSO in breast cancer cells, potentially by reducing glutamate levels and impairing GSH synthesis to a greater degree than BSO alone (Beatty et al., 2017; Biancur et al., 2017). Conversely, it was less clear why *USP7* and *UCHL5* scored as dependencies under conditions of GSH depletion. Validation of USP7 was carried out using distinct sgRNAs against *USP7*, with loss of USP7 sensitizing cells to the effects of GSH depletion (Figures 2F and 2G).

To complement the genetic screening, we designed and assembled a high-throughput compound screening platform in order to interrogate the differential drug sensitivities in cancer cells upon depletion of GSH. Similar methods have been used to determine resistance mechanisms in cancer cells to targeted therapies (Crystal et al., 2014; Vora et al., 2014). A collection of more than 500 compounds targeting not only well-characterized

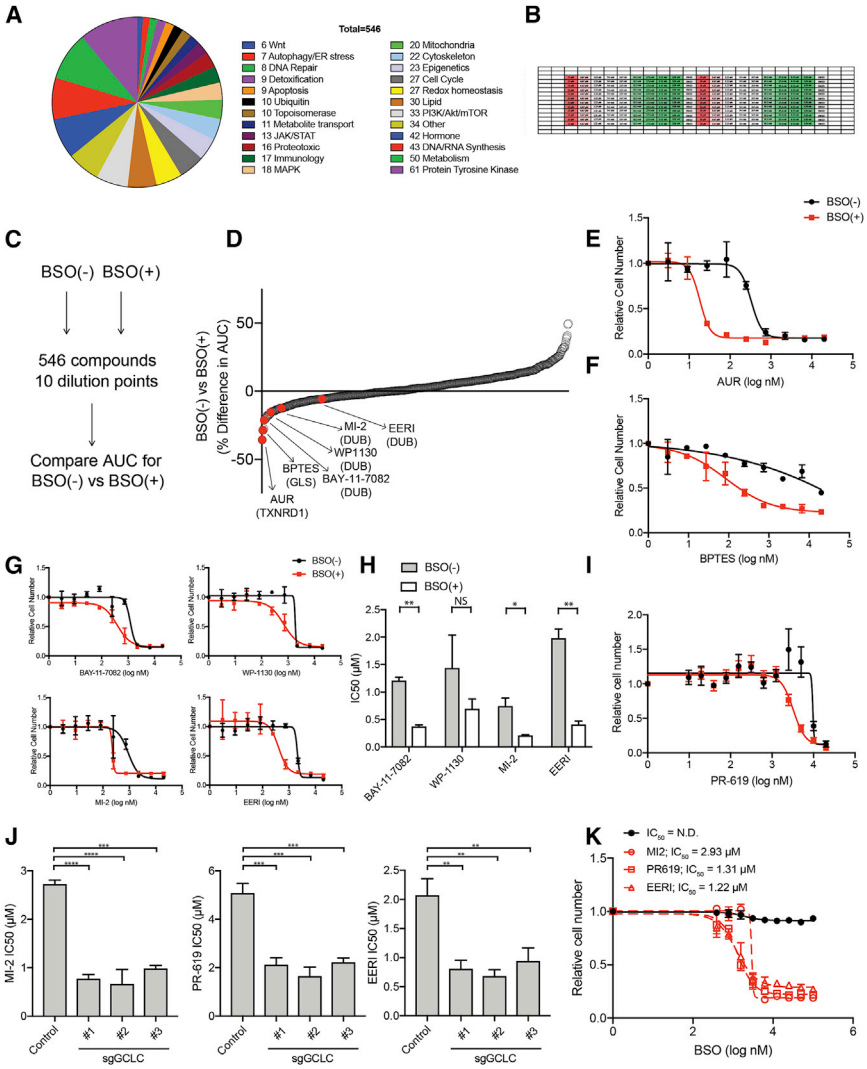

Figure 3. Pharmacologic Screening Reveals DUBs Support Survival of Cancer Cells upon GSH Depletion

(A) Breakdown of the compound library based on the molecular pathway associated with their target.

(B) Layout of compound screening plates and associated concentrations of each compound. Twenty-four compounds were arrayed onto each screening plate across a 10-point dose curve.

(C) HCC-1806 breast cancer cells treated with vehicle or BSO (100 μM) for 24 h followed by addition of the compound library for 72 h.

(D) Percent difference in area under the curve (AUC) for the relative cell numbers from dose-response curves for each compound in the library.

(E and F) Dose-response curves for HCC-1806 cells treated with vehicle or BSO (100 μM) for 24 h followed by addition of (E) TXNRD1 inhibitor auranofin (AUR) and (F) GLS inhibitor BPTES for 72 h. Data shown as mean ± SD from two technical replicates.

(G and H) (G) Dose-response curves and (H) IC_{50} values for HCC-1806 breast cancer cells treated with vehicle or BSO (100 μM) for 24 h followed by addition of DUB inhibitors for 72 h. Data shown as mean ± SD from two technical replicates.

(I) Dose-response curves for HCC-1806 breast cancer cells treated with vehicle or BSO (100 μM) for 24 h followed by addition of DUB inhibitor PR-619 for 72 h. Data shown as mean ± SD from eight technical replicates.

(J) IC_{50} values for control and sgGCLC HCC-1806 breast cancer cells treated with DUB inhibitors for 72 h. Data are represented as mean ± SEM from three independent experiments.

(K) BSO dose-response curve of HCC-1806 breast cancer cells treated with vehicle, MI-2 (1.25 μM), PR-619 (2.5 μM), or EERI (1.25 μM) for 72 h. Data shown as mean ± SD from three technical replicates and representative of two independent experiments. NS, not statistically significant; *$p < 0.05$, **$p < 0.01$, ***$p < 0.001$, ****$p < 0.0001$. Dunnett's multiple comparisons test was used to determined statistical significance for (J). Unpaired two-tailed t test was used to determined statistical significance for (H). See also Figures S2 and S3 and Table S4.

cancer-associated proteins but also metabolic enzymes were arrayed across a 10-point dose curve ranging from 20 μM to 3 nM and screened using an image-based readout (Figures 3A and 3B). The screening platform was used to test the sensitivity of HCC-1806 and MDA-MB-468 breast cancer lines to compounds in the presence of a fixed dose of BSO (100 μM) (Figures 3C, 3D, and S2A; Table S4). Recapitulating previously reported findings (Harris et al., 2015; Mandal et al., 2010), we found that auranofin, an inhibitor of TXNRD1, sensitized cancer cells to inhibition of GCLC as indicated by a decrease in area under the curve (AUC) from the dose-response curve (Figure 3E). An inhibitor of GLS (BPTES) also scored as a hit (Figure 3F), mimicking the genetic screening result. Additionally, we observed sensitization by alkylating agents (e.g., chlorambucil, bendamustine, lomustine, and busulfan) (Table S4); these findings mirror results from phase 1 clinical trials where BSO was combined with the alkylating agent melphalan (NCT00005835 and NCT00002730) (Bailey, 1998; Villablanca et al., 2016). Interestingly, four structurally distinct compounds with activity against DUBs (MI-2, WP1130, BAY-11-7082, and EERI) (Fiebiger et al., 2004; Ritorto et al., 2014; Wang et al., 2008) were among the compounds that sensitized cancer cells to GSH depletion (Figures 3G, 3H, S2B, and S2C). WP1130 and BAY-11-7082 inhibit not only USP7 but also a diverse set of additional DUBs (Ritorto et al., 2014). EERI targets a DUB associated with p97/valosin-containing protein (VCP) and impairs the function of the endoplasmic reticulum (ER)-associated degradation (ERAD) (Wang et al., 2008). MI-2, originally identified as a MALT-1 protease inhibitor (Fontan et al., 2012), was determined to have potent inhibitory activity against multiple DUBs using *in vitro* DUB target engagement assay (Figures S2D and S2E). A pan-DUB inhibitor (PR-619) (Altun et al., 2011) that was not present in our drug library was

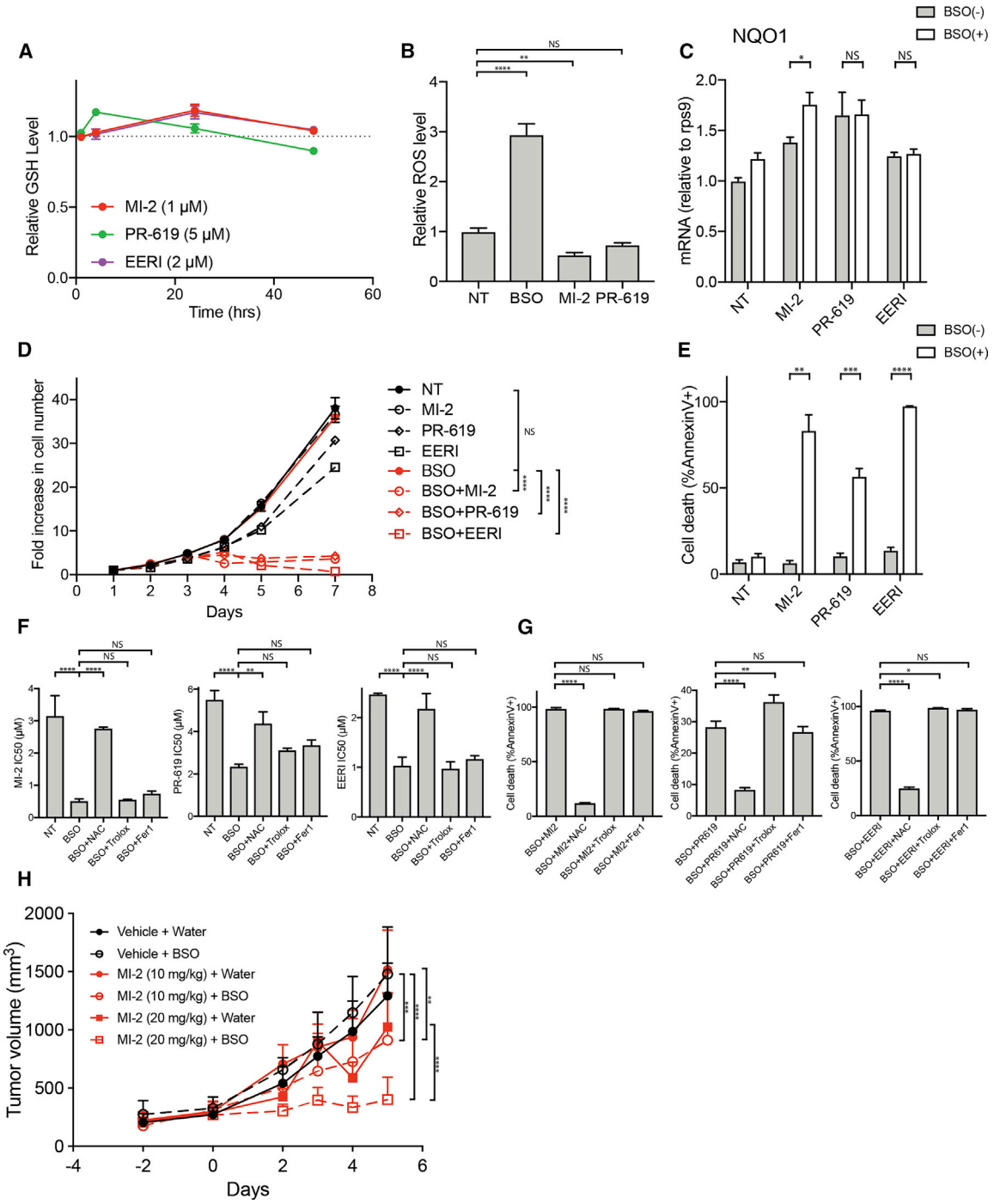

Figure 4. Protein Deubiquitination Contributes to Survival upon Suppression of GSH Synthesis

(A) Relative GSH levels from HCC-1806 breast cancer cells treated with DUB inhibitors for the indicated times. Data shown as mean ± SEM from three independent experiments.

(B) ROS levels from HCC-1806 breast cancer cells treated with BSO (100 μM), MI-2 (1 μM), or PR-619 (5 μM) for 24 h. Data shown as mean ± SD from three technical replicates.

(C) NRF2 target gene *NQO1* mRNA in HCC-1806 breast cancer cells treated with vehicle or BSO (100 μM) for 24 h followed by addition of DUB inhibitors MI-2 (1 μM), PR-619 (5 μM), or EERI (2 μM) with vehicle or BSO (100 μM) for 8 h. Data shown as mean ± SEM from three independent experiments.

(D) Fold increase in cell numbers from day 1 for HCC-1806 breast cancer cells treated as in (C). Data shown as mean ± SD from three technical replicates.

(E) Percent cell death (determined by Annexin V staining) for HCC-1806 breast cancer cells treated as in (C) for 72 h. Data shown as mean ± SEM from three independent experiments.

(legend continued on next page)

tested and found to also sensitize cancer cells to GCLC inhibition (Figure 3I). The impact of simultaneous inhibition of multiple DUB enzymes on the sensitivity of cells to GSH depletion was far greater than the effect observed with deletion of *USP7* alone (Figure 2G).

Two findings ruled out off-target effects of BSO in the drug interactions: (1) deletion of *GCLC* alone (in the absence of BSO) increased the sensitivity of HCC-1806 breast cancer cells to the DUB inhibitors (Figure 3J), and (2) the IC_{50} dose of BSO for inhibition of cell numbers in the context of DUB inhibition matched that for the reduction of intracellular GSH levels (Figures 1F, 1J, and 3K). Furthermore, treatment with sulfasalazine, an inhibitor of the cysteine transporter xCT (Lewerenz et al., 2013), which limits synthesis of GSH by depleting intracellular cysteine levels, similarly sensitized cancer cells to DUB inhibitors (Figure S3A). Because TXNRD1 is known to support cell survival upon GSH depletion, we also assessed whether TXNRD1 activity was reduced in the presence of DUB inhibitors. We found that the DUB inhibitors did not affect TXNRD1 activity *in vitro* or TXN1 oxidation status *in vivo* (Figures S3B–S3D). TXN1 is reduced by TXNRD1 and thus its level of oxidation reflects TXNRD1 activity. These results suggest that the sensitization to BSO induced by DUB inhibition is not due to effects on TXNRD1 activity. In addition, comparable synergistic activities between BSO and DUB inhibition were observed upon CRISPR-Cas9-mediated deletion of *TXNRD1* in HCC-1806 breast cancer cells (Figures S3E and S3F).

Taken together, the data derived from both genetic and pharmacologic screening approaches provide evidence that maintenance of activity in DUBs is required to sustain the survival of cancer cells upon GSH depletion.

Combined Inhibition of GCLC and DUBs Induces Cell Death

To better understand the effect of DUB inhibition on the sensitivity to GCLC inhibition, GSH levels were measured in cancer cells treated with DUB inhibitors. None of the DUB inhibitors reduced GSH levels in HCC-1806 and MDA-MB-468 breast cancer cells (Figures 4A and S4A). Furthermore, DUB inhibition did not increase ROS levels nor elicit a strong NRF2-mediated antioxidant response (based on the expression of two canonical target genes *NQO1* and *GCLC*) (Figures 4B, 4C, and S4B). A time course analysis of treatment with a DUB inhibitor (MI-2, PR-619, or EERI) in combination with BSO demonstrated that these combinations cause a significant inhibition of cell numbers (Figure 4D), and quantification of apoptosis revealed a large increase in cell death (Figure 4E), suggesting that the reduction in cell number observed was predominantly due to a cytotoxic effect. The effect of GCLC inhibition on sensitivity to DUB inhibitors could be rescued with the antioxidants N-acetyl cysteine (NAC) and a cell-permeable GSH ethyl ester (GSHee) (Figures 4F, 4G, and S4C). GSHee rescued the sensitivity to MI-2 and PR-619 in combination with BSO but not EERI. The basis for the lack of rescue with GSHee in cells treated with EERI and BSO is not known but could reflect differences in the nature of EERI responses relative to the other DUB inhibitors since the target of EERI (p97/VCP) regulates cellular complexes other than ERAD and its associated DUBs.

Depletion of GSH in some cell contexts has been shown to lead to ferroptosis, a death process triggered by excessive lipid peroxidation (Dixon et al., 2012). To investigate whether inhibition of DUBs and/or GCLC affected lipid peroxidation, we measured the level of lipid peroxides, which accumulate upon ferroptosis induction, with the C11-BODIPY lipid peroxidation sensor (Figure S4D). We observed an increase in lipid peroxides with combined treatment with BSO and DUB inhibitors in HCC-1806 breast cancer cells but not to the extent observed with a known inducer of ferroptosis (ML-210). To investigate whether this increase in lipid peroxides contributes to the cell death induced by BSO and DUB inhibition, we examined whether agents that relieve lipid peroxidation (Trolox and Ferrostatin-1) rescue the cytotoxicity. We first validated that the experimental doses of Ferrostatin-1 and Trolox adequately blocked ferroptosis, as seen by the rescue of cells treated with RSL3, a GPX4 inhibitor that induces ferroptosis (Figures S4E and S4F). We found that neither Trolox nor Ferrostatin-1 could rescue cells treated with BSO and DUB inhibitors (Figures 4F, 4G, and S4G). These results suggest that while BSO and DUB inhibition induce lipid peroxides, this does not contribute to the cell death observed. Additionally, DUB inhibitors did not sensitize cells to auranofin (Figure S4H), suggesting this sensitivity was specific to GSH depletion and not applicable to the inhibition of the antioxidant TXN. The effect of DUB inhibition on sensitivity to BSO was observed across cell lines derived from multiple tumor types (Figure S4I).

To determine whether this drug combination shows efficacy *in vivo*, we examined the effect of a single agent and combined treatment with BSO and one of the DUB inhibitors (MI-2) in mice carrying HCC-1806 breast cancer cell xenograft tumors. MI-2 has previously shown *in vivo* efficacy in mouse models (Fontan et al., 2012). After palpable tumors were formed ($\sim$300 mm^3), mice were randomized into six treatment arms: (1) vehicle + water, (2) vehicle + BSO, (3) MI-2 (10 mg/kg) + water, (4) MI-2 (10 mg/kg) + BSO, (5) MI-2 (20 mg/kg) + water, and (6) MI-2 (20 mg/kg) + BSO. We found that combined treatment with BSO and 20 mg/kg MI-2 caused a dramatic reduction in

(F) IC_{50} values for HCC-1806 breast cancer cells treated with BSO (100 μM) for 24 h followed by addition of DUB inhibitors and BSO (100 μM) in combination with NAC (5 mM), Trolox (250 μM), or Ferrostatin-1 (1 μM) for 72 h. Data shown as mean ± SD from three technical replicates and representative of three independent experiments.

(G) Percent cell death (determined by Annexin V staining) for HCC-1806 breast cancer cells treated as in (F). Data are represented as mean ± SD from three technical replicates and representative of three independent experiments.

(H) HCC-1806 breast cancer cells were subcutaneously injected into nude mice and allowed to form palpable tumors ($\sim$300 mm^3), and then mice were randomized into six arms (n = 5 mice per arm): (1) vehicle + water, (2) vehicle + BSO, (3) MI-2 (10 mg/kg) + water, (4) MI-2 (10 mg/kg) + BSO, (5) MI-2 (20 mg/kg) + water, and (6) MI-2 (20 mg/kg) + BSO. Tumor dimensions were measured every 1–2 days and volumes were calculated. NT, not treated. NS, not statistically significant; *p < 0.05, **p < 0.01, ***p < 0.001, ****p < 0.0001. Dunnett's multiple comparisons test was used to determined statistical significance for (B), (F), and (G). Unpaired two-tailed t test was used to determined statistical significance for (C), (E), and (H). Two-way ANOVA was used to determined statistical significance for (D). See also Figure S4.

tumor growth compared to vehicle or single agents (Figure 4H). A lower dose of MI-2 in combination with BSO caused a less significant reduction in tumor growth but greater than that of a single agent alone. Importantly, combined treatment with MI-2 and BSO did not cause a more significant reduction in body weight than BSO alone, suggesting that this combination is not highly toxic (Figure S4J).

To investigate the toxicity of the other two DUB inhibitors, PR-619 and EERI (whose solubility properties limited examination *in vivo*), on normal cells, we utilized organoid cultures of human and mouse mammary epithelial cells. These culture conditions preserve cell populations present in mammary glands (Sachs et al., 2018). For these assays, ATP levels were measured (using Cell Titer Glo) and used as a surrogate for cell viability because of the complications in quantifying cell numbers in 3D organoids. We found that treatment of organoids with BSO and PR-619 significantly reduced viability, whereas treatment with BSO and EERI did not significantly reduce viability (Figure S4K). However, the extent of reduction in these normal cells was smaller than the effects on viability observed in our cancer cell lines, where these drug combinations caused >90% reduction in viability. Together, these data support further evaluation of this drug combination in appropriate preclinical models.

DUB Inhibition and GSH Depletion Induce Both Proteotoxic and ER Stress

Since DUBs remove ubiquitin groups from proteins and an accumulation of ubiquitinated proteins can lead to cell death (D'Arcy and Linder, 2014), we measured total protein ubiquitination in cells 8 h after a single agent or combined treatment with BSO and each of the three DUB inhibitors. While neither single agent BSO nor MI-2 nor PR-619 significantly affected protein ubiquitination, combined treatment with BSO and either DUB inhibitor substantially increased ubiquitination (Figures 5A and S5A). EERI, which inhibits ataxin-3-dependent degradation of proteins ubiquitinated by the ERAD complex (Wang et al., 2008), increased the levels of ubiquitinated proteins as a single agent; however, BSO co-treatment enhanced ubiquitination (Figure 5A). The increased effect on protein ubiquitination by EERI as compared to MI-2 and PR-619 could potentially contribute to the inability of GSHee to rescue HCC-1806 cells treated with EERI and BSO (Figure S4C); however, further investigation is required to fully explain this phenotype. The buildup of ubiquitinated proteins in the BSO and DUB inhibitor co-treated cells could potentially impose an excessive burden on the proteasome, leading to proteotoxic stress and stabilization of the transcription factor heat shock factor 1 (HSF1) (Dai et al., 2007; Morimoto, 2008). We observed a rapid increase in mRNA and protein levels of HSF1 target genes when both DUB and GCLC activities were inhibited (Figures 5B, 5C, S5B, and S5C). Proteotoxic stress can also cause ER stress (De Raedt et al., 2011); accordingly, we observed activation of the unfolded protein response (UPR) with combined inhibition of DUB activity and GSH synthesis as measured by increased transcription of *GADD34* and *CHOP* (Hetz et al., 2015), as well as stabilization of the ER protein GRP78 (BIP) and activating transcription factor 4 (ATF4) (Figures 5D and 5E). Upregulation of proteotoxic and ER stress response gene transcription was reversed by addition of NAC (Figure S5D), suggesting that oxidative stress associated with combined DUB inhibition and GSH depletion is critical for the induction of proteotoxic and ER stress in HCC-1806 breast cancer cells. Furthermore, we observed minimal to no change in the pathways involving GSH synthesis, serine synthesis, cysteine uptake, and NRF2 (Figure S5E) upon combined BSO and DUB inhibition. Interestingly, we did observe increased expression of cystathionine gamma-lyase (CTH), a protein responsible for cysteine biosynthesis via the transsulfuration pathway, suggesting that this pathway may support redox buffering directly by cysteine itself (Poole, 2015) or GSH-independent synthesis of antioxidants, such as hypotaurine and taurine, which act as a redox couple (Aruoma et al., 1988), and potentially regulate the cytotoxicity upon BSO and DUB inhibition.

To further understand the contribution of ER stress to the phenotypes observed upon BSO and DUB inhibition, we treated HCC-1806 breast cancer cells with the ER stress-inducing agent tunicamycin in combination with DUB inhibitors (Figure S5F). Treatment with an ER stress inducer significantly reduced the IC_{50} of DUB inhibitors, demonstrating that the induction of ER stress can phenocopy GSH depletion with respect to enhancement of sensitivity to DUB inhibition.

These results suggest that inhibition of DUBs induces proteotoxic stress provoked by GSH depletion and raised the question whether in BSO-sensitive cell lines, single-agent BSO treatment is sufficient to induce high levels of proteotoxic stress. Interestingly, BSO increased transcription of HSF1 and UPR target genes in the absence of DUB inhibition in the BSO-sensitive cell lines, an effect that was minimal or not detected in the resistant cancer cell lines (Figures 5F and 5G). The effect of single-agent BSO in the sensitive cell lines was observed only after an extended time period (7 days) as opposed to the short duration of the combined treatment with BSO and DUB inhibitors (8 h). To determine the level of GSH depletion at which the combined treatment of BSO and DUB inhibition becomes synergistic (combination index; CI < 1), we conducted Chou-Talalay synergy analysis (Chou, 2010) with the DUB inhibitor MI-2 (Figure S5G). We found that treatment with approximately 3 μM BSO, which caused an approximate 12% inhibition of GSH synthesis, resulted in BSO and MI-2 synergistic effects in HCC-1806 breast cancer cells. Overall, this suggests that while blocking GSH synthesis alone leads to an accumulation of proteotoxic stress over time in a subset of BSO-sensitive cell lines, inhibition of GSH renders cancer cells acutely dependent on DUBs to maintain protein homeostasis and support cell viability.

Genetic Screen Reveals Factors Mediating Survival upon GCLC and DUB Inhibition

In order to identify factors that regulate the survival of cells treated with the combined inhibitors, a pooled CRISPR-Cas9 screen was conducted in HCC-1806 breast cancer cells to identify genes that positively or negatively impact survival or proliferation under conditions of BSO and DUB inhibition (using either PR-619 or EERI) (Figures 6A, 6B, and S6A; Table S5). sgRNAs targeting X-linked inhibitor of apoptosis (*XIAP*) were the strongest hits among the sgRNAs that dropped out in DUB/GCLC-inhibitor-treated cells relative to GCLC inhibition alone (Figures 6B, 6C, S6A, and S6B). Another anti-apoptotic protein, BCL-XL (*BCL2L1*), was also a top hit from the screen. Interestingly,

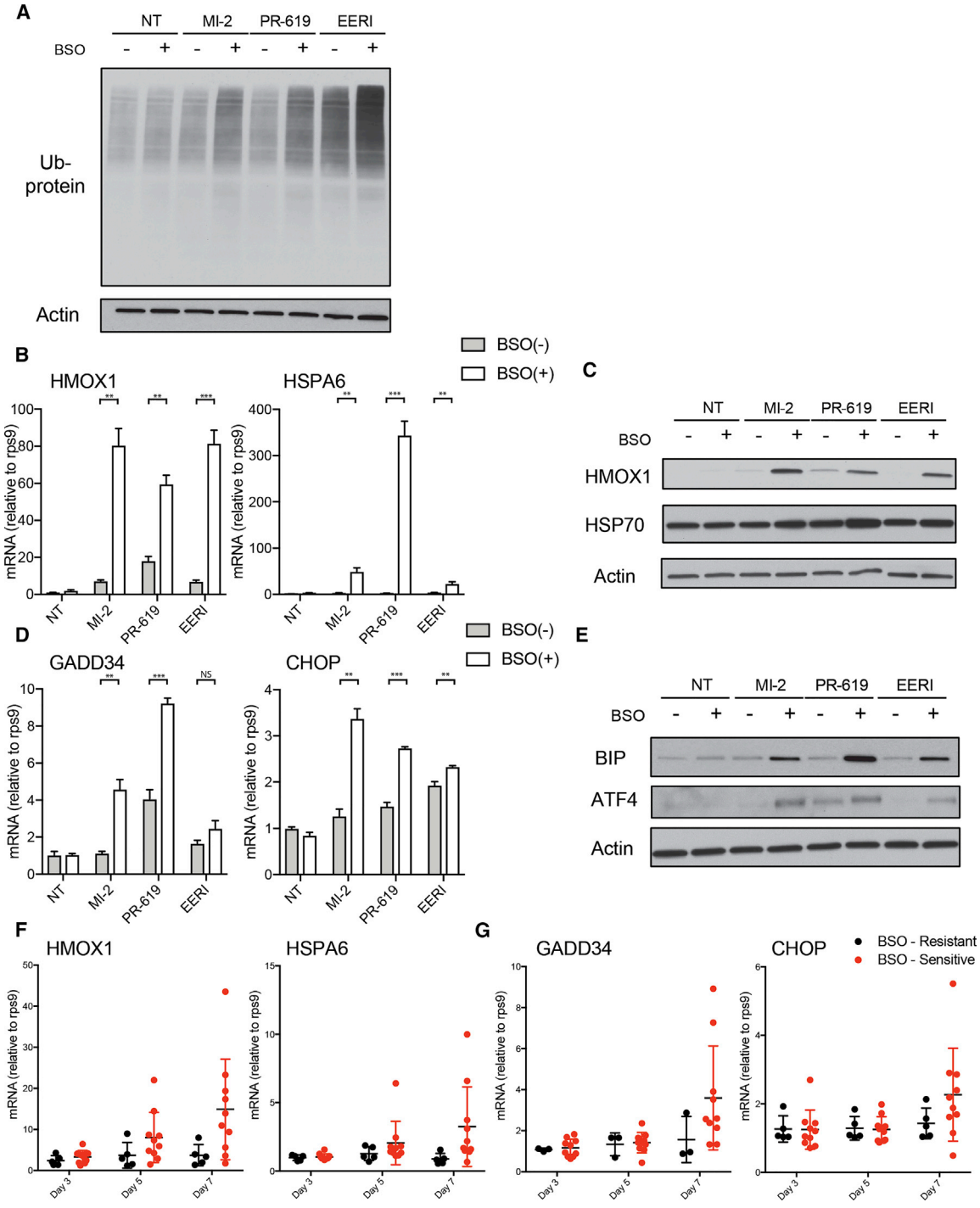

Figure 5. Combined DUB and GCLC Inhibition Leads to Proteotoxic and ER Stress

(A) Representative immunoblot analysis of total ubiquitinated proteins in HCC-1806 breast cancer cells treated with vehicle or BSO (100 μM) for 24 h followed by addition of DUB inhibitors MI-2 (1 μM), PR-619 (5 μM), or EERI (2 μM) with vehicle or BSO (100 μM) for 8 h.

(B and C) (B) HSF1 target gene mRNA and (C) representative immunoblot analysis of target proteins in HCC-1806 breast cancer cells treated as in (A). Data shown as mean ± SEM from three independent experiments.

(D and E) (D) UPR target gene mRNA and (E) representative immunoblot analysis of target proteins in HCC-1806 breast cancer cells treated as in (A). Data shown as mean ± SEM from three independent experiments.

(F and G) (F) HSF1 and (G) UPR target gene mRNA in BSO-resistant (n = 5) and BSO-sensitive (n = 10) breast cancer cell lines treated with BSO (100 μM) for 7 days (media with vehicle and BSO replenished every 48 h). Data shown as mean ± SD from three technical replicates. NT, not treated. NS, not statistically significant; *p < 0.05, **p < 0.01, ***p < 0.001. Unpaired two-tailed t test was used to determine statistical significance. See also Figure S5.

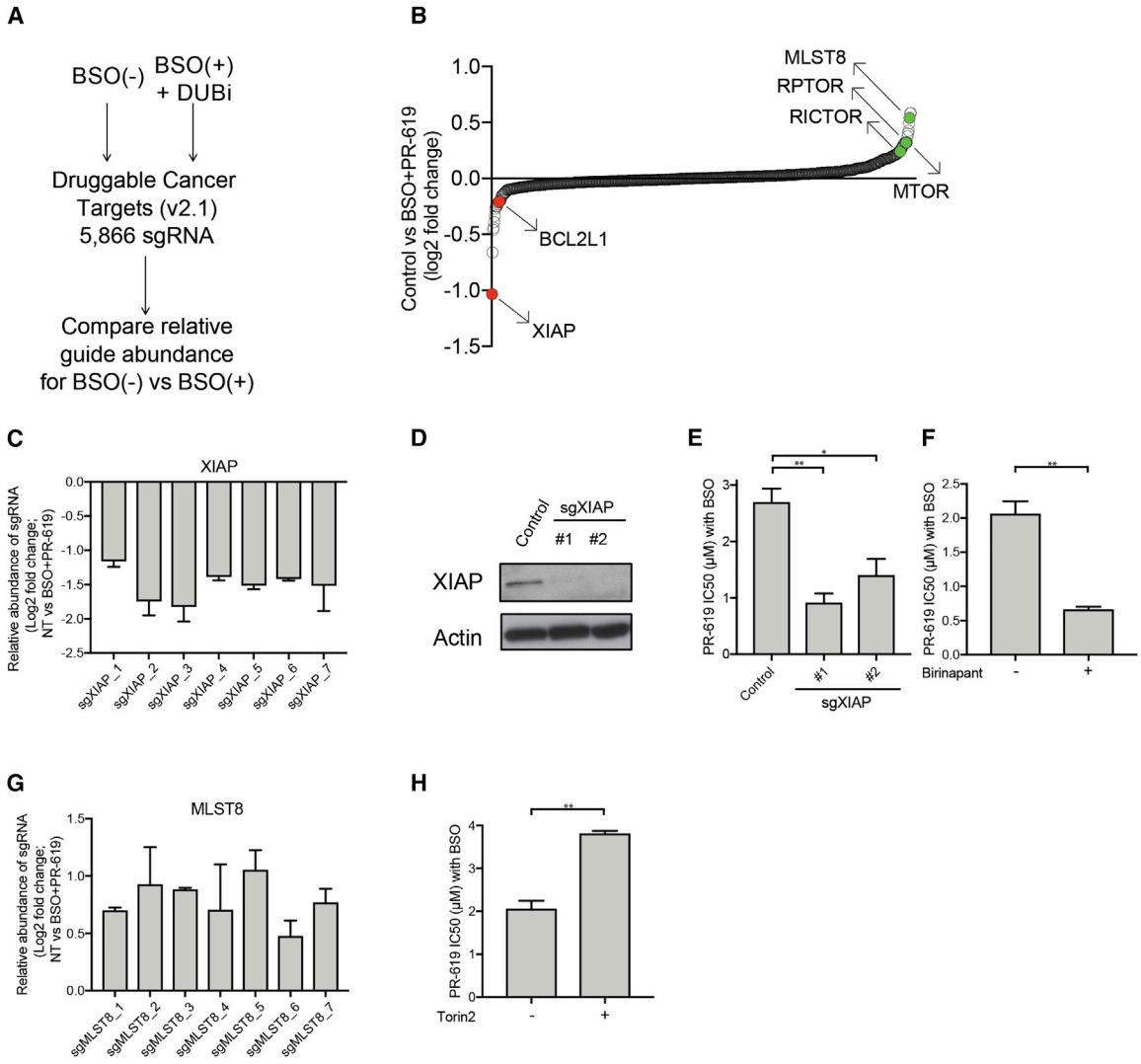

Figure 6. Anti-apoptotic Proteins and mTOR Signaling Dictate Survival under Conditions of Combined Inhibition of GCLC and DUBs

(A) Schematic of genetic screening of HCC-1806 breast cancer cells with pooled CRISPR library against "druggable" genes treated with BSO (100 μM) and DUB inhibitor PR-619 (5 μM).

(B and C) Relative sgRNA guide abundance for (B) the entire library and sgRNAs against (C) *XIAP* for HCC-1806 breast cancer cells treated with vehicle or BSO (100 μM) and DUB inhibitor PR-619 (5 μM) for 16 days. Data shown as mean ± SD of two technical replicates.

(D) Representative immunoblot analysis of XIAP protein in HCC-1806 breast cancer cells transduced with LentiCrisprV2 with control sgRNA or sgRNA targeting *XIAP*.

(E) IC_{50} values for control and sgXIAP HCC-1806 breast cancer cells treated with BSO (100 μM) for 24 h followed by addition of PR-619 for 72 h. Data shown as mean ± SEM from three independent experiments.

(F) IC_{50} values for HCC-1806 breast cancer cells treated with or without BSO (100 μM) and pan-inhibitor of IAPs birinapant (500 nM) for 24 h followed by addition of PR-619 for 72 h. Data shown as mean ± SEM from three independent experiments.

(G) Relative sgRNA guide abundance for sgRNAs against *MLST8* for HCC-1806 breast cancer cells treated as in (B) and (C). Data shown as mean ± SD from two technical replicates.

(H) IC_{50} values for HCC-1806 breast cancer cells treated with or without BSO (100 μM) and mTORC kinase inhibitor Torin2 (500 nM) for 24 h followed by addition of PR-619 for 72 h. Data shown as mean ± SEM from three independent experiments. *$p < 0.05$, **$p < 0.01$. Dunnett's multiple comparisons test was used to determined statistical significance for (E). Unpaired two-tailed t test was used to determined statistical significance for (F)–(H). See also Figure S6 and Table S5.

XIAP has previously been found to be regulated by components of the UPR, with ATF4 promoting degradation of XIAP, thus causing increased apoptosis upon chronic ER stress (Hiramatsu et al., 2014). Deletion of XIAP using independent sgRNAs sensitized cells to the combined inhibition of GSH synthesis and DUB activity (Figures 6D and 6E), validating XIAP as a regulator of survival in this context. Furthermore, this phenotype could be recapitulated using the compound birinapant, a pan-IAP antagonist (Benetatos et al., 2014) (Figure 6F). Overall, these results suggest that the sensitivity to GSH depletion imparted by DUB inhibition forces the cancer cell to rely on anti-apoptotic proteins to support survival.

Interestingly, cells with sgRNAs targeting components of mTORC1/2 were found to be enriched in cells treated with GCLC and DUB inhibitors (Figures 6B, 6G, S6A, and S6C). Increased protein synthesis through the mTOR pathway has been shown to promote ER stress (Ozcan et al., 2008), suggesting that hyperactivation of this pathway, which is observed in numerous tumors (Guertin and Sabatini, 2007), may further sensitize cancer cells to inhibition of GSH and DUB pathways. mTOR activity was validated as a negative regulator of cell survival in this context by the finding that Torin2, a potent inhibitor of mTOR kinase activity (Liu et al., 2013), rendered cells less sensitive to combined DUB and GCLC inhibition (Figures 6H and S6D).

DISCUSSION

GSH, the most abundant cellular antioxidant, has been implicated in the regulation of many processes associated with tumor progression and sensitivity to cancer therapy. We undertook an effort to systematically analyze the consequences of inhibiting GCLC, the rate-limiting enzyme in GSH synthesis, in cancer cells. Under standard cell culture conditions, we found GSH to be dispensable in the majority of cancer cell lines examined. Using unbiased genetic and pharmacologic screening approaches, we found that GSH becomes indispensable when the activity of DUBs is impaired. Furthermore, the combined inhibition of GCLC and DUBs in cancer cells caused an accumulation of proteotoxic and ER stress and cell death. Additional genetic screening revealed the involvement of anti-apoptotic proteins as well as signaling pathways that regulate protein synthesis in regulating the sensitivity to combined GSH and DUB inhibition.

Reduced GSH levels have been implicated in cancer cell death in response to a variety of conditions (Trachootham et al., 2009), e.g., inhibition of cystine uptake (Yang et al., 2014) and disruption of NADPH homeostasis (Wang et al., 2017). However, our study demonstrates that depletion of GSH is not sufficient to induce cell death in most cancer cell lines. In the subset of cell lines where GSH depletion was sufficient to cause cell death, cytotoxicity occurred after prolonged GSH depletion and was associated with proteotoxic and ER stress. These results support previous findings indicating that most tumor cells adapt robust mechanisms to tolerate oxidative stress (Gill et al., 2016; Maddocks et al., 2013)

The screens performed in this study surveyed a broad spectrum of perturbations to identify factors that render cancer cells dependent on GSH and demonstrated that inhibition of DUBs impedes cells from tolerating depletion of GSH. DUB-mediated protection from GSH depletion represents a previously unrecognized mechanism for adaptation to oxidative stress. While the precise mechanism involved in DUB-mediated oxidative stress tolerance is unknown, it is likely to involve DUB-mediated reduction in the accumulation of ubiquitinated proteins that result from oxidation-induced protein misfolding. Recent studies have demonstrated that a wide range of proteins, both of high and low abundance and across numerous cellular compartments, becomes oxidized at cysteine residues under conditions that increase intracellular ROS levels (van der Reest et al., 2018), as well as upon depletion of tumor-promoting proteins that modulate oxidative stress, such as NRF2 (Bar-Peled et al., 2017; Chio et al., 2016). Proteins that are misfolded by cysteine oxidation would be marked for ubiquitination; excess levels of ubiquitinated proteins would put extra demand on DUBs to either promote proteasomal degradation of toxic misfolded proteins or to rescue ubiquitinated proteins from degradation (Komander et al., 2009) and provide an opportunity for refolding (Braakman and Bulleid, 2011).

GSH plays a particularly critical role in maintaining the redox balance in the highly oxidized environment of the ER (Birk et al., 2013). Compared with other organelles, the ratio of reduced to oxidized GSH is much lower in the ER (Hwang et al., 1992) due to the requirement for oxidized cysteines to mediate proper protein folding. Indeed, inhibition of GSH synthesis leads to increased oxidation of the ER prior to changes in the cytosol (Melo et al., 2017). EERI, a top-scoring compound from the pharmacologic screen, inhibits p97/VCP, which has also been shown to play roles outside of the ER, including the regulation of ribosome quality control (Brandman and Hegde, 2016; Meyer et al., 2012) and chromatin complexes (Ramadan et al., 2007).

It is likely that the inhibition of multiple DUBs contributes to the toxicity of combined DUB and GCLC suppression. Large-scale mass spectrometry analyses have provided information on the specificities of cellular DUBs as well as their interacting proteins and candidate targets (Ritorto et al., 2014; Sowa et al., 2009). These studies, together with more specific studies of individual DUBs (Mevissen and Komander, 2017), have provided evidence that a large subset of DUBs has a limited number of specific targets that regulate many cellular processes, such as CYLD, which regulates NFκB signaling (Sun, 2008), and USP9X, which regulates apoptosis by deubiquitinating the anti-apoptotic protein MCL-1 (Schwickart et al., 2010). Other DUBs such as USP14, UCHL5, PSMD7, and PSMD14 are directly associated with the proteasome and affect overall protein degradation (Harrigan et al., 2018). Our CRISPR-Cas9 genetic screen revealed that deletion of *USP7* or *UCHL5* weakly sensitized HCC-1806 breast cancer cells to GSH depletion. USP7 is associated with multiple protein complexes involved in diverse cellular activities (Nicholson and Suresh Kumar, 2011). Since USP7 targets numerous proteins for deubiquitination, loss of this DUB could lead to an overall buildup of ubiquitinated proteins. Another factor potentially contributing to the increased sensitivity of cancer cells to DUB inhibition upon GSH depletion is the generation of ROS that occurs under this condition. ROS inactivate many DUBs, including USP7 and UCHL5 (Cotto-Rios et al., 2012; Lee et al., 2013), through oxidation of active site reactive cysteines. Thus, depletion of GSH could cause a general reduction in cellular DUB activity, which is then exacerbated by either genetic or pharmacologic DUB inhibition and leads to an accumulation of ubiquitinated proteins. This reasoning could explain why compounds that inhibit multiple DUBs scored highly in our pharmacologic screens involving GSH depletion (Ritorto et al., 2014). Genetic deletion of multiple DUBs using combinatorial CRISPR-Cas9 screening techniques (Adamson et al., 2016; Han et al., 2017; Najm et al., 2018) may shed light on which sets of DUBs play more significant roles in buffering the effects of excess protein ubiquitination under conditions of GSH depletion.

Interestingly, both genetic and pharmacologic screens revealed that BSO caused an increased sensitivity to the inhibition of *de novo* lipogenesis controlled by fatty acid synthetase (FASN)

(Tables S3 and S4). Fatty acid synthesis depends on the reducing capacity of NADPH (Wakil and Abu-Elheiga, 2009). One potential explanation for the sensitivity to FASN inhibition upon GSH depletion is that NADPH is diverted away from fatty acid synthesis toward pathways that regulate oxidative stress, such as TXNRD1. Furthermore, hyperactivation of NRF2 has been shown to transcriptionally repress *FASN* mRNA levels (Wu et al., 2011). Further investigations are required to better understand the connections between FASN and GSH synthesis in cancer cells.

Our genetic screening also implicated the mTOR pathway in sensitivity of HCC-1806 and MDA-MB-468 breast cancer cells to combined inhibition of GCLC and DUBs. The mTOR pathway plays a central role in controlling the translation of proteins (Gingras et al., 2001; Ma and Blenis, 2009). Interestingly, components of the mTOR pathway were found to be among the most abundantly oxidized proteins under GSH depletion or under oxidative stress induced from the inhibition of NRF2 (Chio et al., 2016). The rescue of survival of cells under the combined inhibition of DUBs and GSH synthesis could be due to decreased protein synthesis, thus reducing the buildup of ubiquitinated proteins and proteotoxic stress. In addition, since mTOR inhibits autophagy (Kim and Guan, 2015), reduced mTOR activity would allow for increased autophagic processing of ubiquitinated proteins and would promote protein homeostasis and survival of cancer cells upon combined inhibition of GCLC and DUBs. Extrapolating from this, one would predict that tumors with mutations that lead to increased activity of the mTOR pathway would be more sensitive to combined inhibition of GSH synthesis and DUBs (Guertin and Sabatini, 2007).

Changes in the state of a cancer cell, via either epithelial-mesenchymal transition (Viswanathan et al., 2017) or acquired tolerance to targeted therapies (Hangauer et al., 2017), have been associated with increased sensitivity to lipid peroxidation. In the cancer cell lines examined in our study, cell death observed after inhibition of GCLC and DUBs was not due to aberrant lipid peroxidation as indicated by the inability of lipid-targeted antioxidants (Ferrostatin-1 or Trolox) to rescue viability. The evidence that XIAP and BCL-XL were dependencies in the GCLC- and DUB-inhibited HCC-1806 breast cancer cells suggests that apoptotic programs are engaged under these conditions. A more comprehensive examination across a larger number of cancer cell lines is required to provide a better understanding of the death processes associated with distinct sources of oxidative stress and cellular factors that modulate these processes.

Tumor cells are subjected to multiple stresses during initiation and progression of tumorigenesis (Luo et al., 2009), and they co-opt highly conserved programs to adapt to these conditions. These stresses include, but are not limited to, oxidative stress (Chandel and Tuveson, 2014), ER stress (Wang and Kaufman, 2014), and proteotoxic stress (Dai, 2018; Whitesell and Lindquist, 2005). Our study provides evidence for the close integration of programs that regulate protein homeostasis (the rate of protein synthesis and degradation and the machinery that regulates these processes, such as chaperones, ubiquitin ligases, and DUBs; Harper and Bennett, 2016) with processes that control redox homeostasis. Further investigations at single-cell, tissue, and systemic levels are required to better understand the factors that facilitate adaptation of tumors to ER, proteotoxic, and oxidative stress and whether they evolve sequentially or in unison during tumor initiation and progression.

Induction of proteotoxic stress in tumors by directly inhibiting the proteasome has yielded clinical benefits for certain tumor types, such as multiple myeloma, possibly owing to the inherently high rate of protein synthesis in this plasma cell malignancy (Adams, 2004). Targeting DUBs to induce an accumulation of polyubiquitinated proteins and proteotoxic stress has been proposed as an approach to treat cancers (Bedford et al., 2011; D'Arcy and Linder, 2014; Harrigan et al., 2018). Inhibiting DUBs associated with the proteasome (USP14 and UCHL5) with the compound b-AP15 has shown efficacy in blunting tumor growth in pre-clinical models (D'Arcy et al., 2011), but a phase I clinical trial of a derivative of b-AP15 (VLX1570) in combination with dexamethasone for multiple myeloma was terminated because of dose-limiting toxicity (NCT02372240). Targeting of PSMD14, another proteasome-associated DUB, has been recently developed and demonstrates anti-proliferative activity in cancer cells (Lauinger et al., 2017; Li et al., 2017). In the present study, systematic analyses and screening revealed that broad inhibition of DUBs sensitizes cancer cells to depletion of GSH, leading to proteotoxic stress and cell death. We propose that combined inhibition of GCLC and DUBs has the potential for therapeutic benefits.

Limitations of Study

A constraint of using high-throughput screening approaches to interrogate the differential vulnerabilities in cancer cells upon inhibition of GSH synthesis is the necessity to utilize *in vitro* culture models. While the same medium (RPMI 1640) was used throughout our *in vitro* studies, and our findings were recapitulated using a tumor xenograft model, this study warrants further exploration using more relevant tumor models, in particular genetically engineered mouse models (GEMMs) or patient-derived xenografts (PDXs). Another caveat of our study was that we chose to investigate only a subset of compounds and genes for our screens since this allowed us to test multiple experimental conditions, including a broad span of drug concentrations. A genome-wide genetic screen or utilization of a large, structurally diverse chemical library may yield novel proteins or pathways that would provide new insights into the mediators of resistance in cancer cells upon GSH inhibition. Finally, a limitation existed in defining the specific deubiquitinase (or group of deubiquitinases) involved in the protection of cancer cells against depletion of GSH. A detailed mechanistic investigation into the deubiquitinases involved in this protection could produce novel drug targets that could then potentially be combined with inhibition of GSH synthesis in tumors.

STAR★METHODS

Detailed methods are provided in the online version of this paper and include the following:

- KEY RESOURCES TABLE
- CONTACT FOR REAGENT AND RESOURCE SHARING
- EXPERIMENTAL MODEL AND SUBJECT DETAILS
  - Animal Studies
  - Cell Culture

SUPPLEMENTAL INFORMATION

Supplemental Information includes six figures and six tables and can be found with this article online at https://doi.org/10.1016/j.cmet.2019.01.020.

ACKNOWLEDGMENTS

We would like to thank Alexander Muir, Ed Schmidt, and Angie Martinez Gakidis for critical reading of the manuscript. We would also like to thank Jennifer Smith, Caroline Shamu, and the entire staff at the ICCB-L for their assistance in the chemical screening. This work was supported by the Susan G. Komen for the Cure Foundation (SAC170002, J.S.B.), the Ludwig Center at Harvard (J.S.B.), Canadian Institutes of Health Research (I.S.H.), American Cancer Society MRSG-18-202-01-TBG (A.L.H.), Claudia Adams Barr Program (S.J.B.), NCI grant U01CA176058 (W.C.H.), NIH grant R37CA230042 (G.M.D.), NIH grant R35CA210068-02 (W.G.K.), and Howard Hughes Medical Institute (W.G.K.).

AUTHOR CONTRIBUTIONS

I.S.H. and J.S.B. initiated the study and conceived the project, designed experiments, interpreted results, and wrote the manuscript. I.S.H. performed the experiments with assistance from J.E.E. for high-throughput screening and validation of hits. J.L.C. and L.M.S. carried out bioinformatics analyses; J.M.R., human and mouse mammary organoid experiments; N.T., measuring of lipid peroxidation; S.D., xenograft experiments; Y.P.K. and G.M.D., TXN1 oxidation analysis; S.K.M., V.K., M.G.O., A.L.H., S.T.Y., J.G.D., W.C.H., and W.G.K., CRISPR-Cas9 experiments involving genetic screening; and N.J.S., L.M.D., and S.J.B., DUB engagement assay.

DECLARATION OF INTERESTS

J.S.B. receives funding from F. Hoffmann-La Roche Ltd and is a member of the Scientific Advisory Board (SAB) for eFFECTOR Therapeutics and Agios Pharmaceuticals. J.G.D. is a consultant to Tango Therapeutics. W.C.H. is a consultant to Thermo Fisher, AjuIB, Paraxel, and MPM Capital and is a founder and a member of the SAB for KSQ Therapeutics. W.C.H. receives funding from Deerfield. W.G.K. has financial interests related to Lilly Pharmaceuticals (Board of Directors), Agios Pharmaceuticals (SAB), Cedilla Therapeutics (Founder), FibroGen (SAB), Nextech Invest (SAB), Peloton Therapeutics (SAB), Tango Therapeutics (Founder), and Tracon Pharmaceuticals (SAB). W.G.K. is a coinventor on a patent entitled "Pharmaceuticals and Methods for Treating Hypoxia and Screening Methods Therefor" that has been licensed to FibroGen.

Received: July 1, 2018
Revised: November 30, 2018
Accepted: January 23, 2019
Published: February 21, 2019

REFERENCES

Adams, J. (2004). The development of proteasome inhibitors as anticancer drugs. Cancer Cell *5*, 417–421.

Adamson, B., Norman, T.M., Jost, M., Cho, M.Y., Nuñez, J.K., Chen, Y., Villalta, J.E., Gilbert, L.A., Horlbeck, M.A., Hein, M.Y., et al. (2016). A multiplexed single-cell CRISPR screening platform enables systematic dissection of the unfolded protein response. Cell *167*, 1867–1882.e21.

Altun, M., Kramer, H.B., Willems, L.I., McDermott, J.L., Leach, C.A., Goldenberg, S.J., Kumar, K.G.S., Konietzny, R., Fischer, R., Kogan, E., et al. (2011). Activity-based chemical proteomics accelerates inhibitor development for deubiquitylating enzymes. Chem. Biol. *18*, 1401–1412.

Arrick, B.A., Nathan, C.F., Griffith, O.W., and Cohn, Z.A. (1982). Glutathione depletion sensitizes tumor cells to oxidative cytolysis. J. Biol. Chem. *257*, 1231–1237.

Aruoma, O.I., Halliwell, B., Hoey, B.M., and Butler, J. (1988). The antioxidant action of taurine, hypotaurine and their metabolic precursors. Biochem. J. *256*, 251–255.

Bailey, H.H. (1998). L-S,R-buthionine sulfoximine: historical development and clinical issues. Chem. Biol. Interact. *111–112*, 239–254.

Bar-Peled, L., Kemper, E.K., Suciu, R.M., Vinogradova, E.V., Backus, K.M., Horning, B.D., Paul, T.A., Ichu, T.-A., Svensson, R.U., Olucha, J., et al. (2017). Chemical proteomics identifies druggable vulnerabilities in a genetically defined cancer. Cell *171*, 696–709.e23.

Barretina, J., Caponigro, G., Stransky, N., Venkatesan, K., Margolin, A.A., Kim, S., Wilson, C.J., Lehar, J., Kryukov, G.V., Sonkin, D., et al. (2012). The Cancer Cell Line Encyclopedia enables predictive modelling of anticancer drug sensitivity. Nature *483*, 603–607.

Beatty, A., Fink, L.S., Singh, T., Strigun, A., Peter, E., Ferrer, C.M., Nicolas, E., Cai, K.Q., Moran, T.P., Reginato, M.J., et al. (2017). Metabolite profiling reveals the glutathione biosynthetic pathway as a therapeutic target in triple negative breast cancer. Mol. Cancer Ther. *17*, 264–275.

Bedford, L., Lowe, J., Dick, L.R., Mayer, R.J., and Brownell, J.E. (2011). Ubiquitin-like protein conjugation and the ubiquitin-proteasome system as drug targets. Nat. Rev. Drug Discov. *10*, 29–46.

Benetatos, C.A., Mitsuuchi, Y., Burns, J.M., Neiman, E.M., Condon, S.M., Yu, G., Seipel, M.E., Kapoor, G.S., Laporte, M.G., Rippin, S.R., et al. (2014). Birinapant (TL32711), a bivalent SMAC mimetic, targets TRAF2-associated cIAPs, abrogates TNF-induced NF-kappaB activation, and is active in patient-derived xenograft models. Mol. Cancer Ther. *13*, 867–879.

Biancur, D.E., Paulo, J.A., Małachowska, B., Del Rey, M.Q., Sousa, C.M., Wang, X., Sohn, A.S.W., Chu, G.C., Gygi, S.P., Harper, J.W., et al. (2017). Compensatory metabolic networks in pancreatic cancers upon perturbation of glutamine metabolism. Nat. Commun. *8*, 15965.

Birk, J., Meyer, M., Aller, I., Hansen, H.G., Odermatt, A., Dick, T.P., Meyer, A.J., and Appenzeller-Herzog, C. (2013). Endoplasmic reticulum: reduced and oxidized glutathione revisited. J. Cell Sci. *126*, 1604–1617.

Braakman, I., and Bulleid, N.J. (2011). Protein folding and modification in the mammalian endoplasmic reticulum. Annu. Rev. Biochem. *80*, 71–99.

Brandman, O., and Hegde, R.S. (2016). Ribosome-associated protein quality control. Nat. Struct. Mol. Biol. *23*, 7–15.

Cancer Cell Line Encyclopedia Consortium; Genomics of Drug Sensitivity in Cancer Consortium (2015). Pharmacogenomic agreement between two cancer cell line data sets. Nature *528*, 84–87.

Chandel, N.S., and Tuveson, D.A. (2014). The promise and perils of antioxidants for cancer patients. N. Engl. J. Med. *371*, 177–178.

Chio, I.I.C., Jafarnejad, S.M., Ponz-Sarvise, M., Park, Y., Rivera, K., Palm, W., Wilson, J., Sangar, V., Hao, Y., Öhlund, D., et al. (2016). NRF2 promotes tumor maintenance by modulating mRNA translation in pancreatic cancer. Cell *66*, 963–976.

Chio, I.I.C., and Tuveson, D.A. (2017). ROS in cancer: the burning question. Trends Mol. Med. *23*, 411–429.

Chou, T.C. (2010). Drug combination studies and their synergy quantification using the Chou-Talalay method. Cancer Res. *70*, 440–446.

Cotto-Rios, X.M., Békés, M., Chapman, J., Ueberheide, B., and Huang, T.T. (2012). Deubiquitinases as a signaling target of oxidative stress. Cell Rep. *2*, 1475–1484.

Crystal, A.S., Shaw, A.T., Sequist, L.V., Friboulet, L., Niederst, M.J., Lockerman, E.L., Frias, R.L., Gainor, J.F., Amzallag, A., Greninger, P., et al. (2014). Patient-derived models of acquired resistance can identify effective drug combinations for cancer. Science *346*, 1480–1486.

D'Arcy, P., Brnjic, S., Olofsson, M.H., Fryknäs, M., Lindsten, K., De Cesare, M., Perego, P., Sadeghi, B., Hassan, M., Larsson, R., et al. (2011). Inhibition of proteasome deubiquitinating activity as a new cancer therapy. Nat. Med. *17*, 1636–1640.

D'Arcy, P., and Linder, S. (2014). Molecular pathways: translational potential of deubiquitinases as drug targets. Clin. Cancer Res. *20*, 3908–3914.

Dai, C. (2018). The heat-shock, or HSF1-mediated proteotoxic stress, response in cancer: from proteomic stability to oncogenesis. Phil. Trans R. Soc. Lond. B. Biol. Sci. *373*.

Dai, C., Whitesell, L., Rogers, A.B., and Lindquist, S. (2007). Heat shock factor 1 is a powerful multifaceted modifier of carcinogenesis. Cell *130*, 1005–1018.

De Raedt, T., Walton, Z., Yecies, J.L., Li, D., Chen, Y., Malone, C.F., Maertens, O., Jeong, S.M., Bronson, R.T., Lebleu, V., et al. (2011). Exploiting cancer cell vulnerabilities to develop a combination therapy for ras-driven tumors. Cancer Cell *20*, 400–413.

DeNicola, G.M., Karreth, F.A., Humpton, T.J., Gopinathan, A., Wei, C., Frese, K., Mangal, D., Yu, K.H., Yeo, C.J., Calhoun, E.S., et al. (2011). Oncogene-induced Nrf2 transcription promotes ROS detoxification and tumorigenesis. Nature *475*, 106–109.

Dixon, S.J., Lemberg, K.M., Lamprecht, M.R., Skouta, R., Zaitsev, E.M., Gleason, C.E., Patel, D.N., Bauer, A.J., Cantley, A.M., Yang, W.S., et al. (2012). Ferroptosis: an iron-dependent form of nonapoptotic cell death. Cell *149*, 1060–1072.

Doench, J.G., Fusi, N., Sullender, M., Hegde, M., Vaimberg, E.W., Donovan, K.F., Smith, I., Tothova, Z., Wilen, C., Orchard, R., et al. (2016). Optimized sgRNA design to maximize activity and minimize off-target effects of CRISPR-Cas9. Nat. Biotechnol. *34*, 184–191.

Du, Y., Zhang, H., Zhang, X., Lu, J., and Holmgren, A. (2013). Thioredoxin 1 is inactivated due to oxidation induced by peroxiredoxin under oxidative stress and reactivated by the glutaredoxin system. J. Biol. Chem. *288*, 32241–32247.

Eriksson, S.E., Prast-Nielsen, S., Flaberg, E., Szekely, L., and Arnér, E.S. (2009). High levels of thioredoxin reductase 1 modulate drug-specific cytotoxic efficacy. Free Radic. Biol. Med. *47*, 1661–1671.

Fiebiger, E., Hirsch, C., Vyas, J.M., Gordon, E., Ploegh, H.L., and Tortorella, D. (2004). Dissection of the dislocation pathway for type I membrane proteins with a new small molecule inhibitor, eeyarestatin. Mol. Biol. Cell *15*, 1635–1646.

Fontan, L., Yang, C., Kabaleeswaran, V., Volpon, L., Osborne, M.J., Beltran, E., Garcia, M., Cerchietti, L., Shaknovich, R., Yang, S.N., et al. (2012). MALT1 small molecule inhibitors specifically suppress ABC-DLBCL in vitro and in vivo. Cancer Cell *22*, 812–824.

Garnett, M.J., Edelman, E.J., Heidorn, S.J., Greenman, C.D., Dastur, A., Lau, K.W., Greninger, P., Thompson, I.R., Luo, X., Soares, J., et al. (2012). Systematic identification of genomic markers of drug sensitivity in cancer cells. Nature *483*, 570–575.

Gill, J.G., Piskounova, E., and Morrison, S.J. (2016). Cancer, oxidative stress, and metastasis. Cold Spring Harb. Symp. Quant. Biol. *81*, 163–175.

Gingras, A.C., Raught, B., and Sonenberg, N. (2001). Regulation of translation initiation by FRAP/mTOR. Genes Dev. *15*, 807–826.

Glasauer, A., Sena, L.A., Diebold, L.P., Mazar, A.P., and Chandel, N.S. (2014). Targeting SOD1 reduces experimental non-small-cell lung cancer. J. Clin. Invest. *124*, 117–128.

Griffith, O.W., and Meister, A. (1979). Potent and specific inhibition of glutathione synthesis by buthionine sulfoximine (S-n-butyl homocysteine sulfoximine). J. Biol. Chem. *254*, 7558–7560.

Guertin, D.A., and Sabatini, D.M. (2007). Defining the role of mTOR in cancer. Cancer Cell *12*, 9–22.

Hakimi, A.A., Reznik, E., Lee, C.-H., Creighton, C.J., Brannon, A.R., Luna, A., Aksoy, B.A., Liu, E.M., Shen, R., Lee, W., et al. (2016). An integrated metabolic atlas of clear cell renal cell carcinoma. Cancer Cell *29*, 104–116.

Han, K., Jeng, E.E., Hess, G.T., Morgens, D.W., Li, A., and Bassik, M.C. (2017). Synergistic drug combinations for cancer identified in a CRISPR screen for pairwise genetic interactions. Nat. Biotechnol. *35*, 463–474.

Hangauer, M.J., Viswanathan, V.S., Ryan, M.J., Bole, D., Eaton, J.K., Matov, A., Galeas, J., Dhruv, H.D., Berens, M.E., Schreiber, S.L., et al. (2017). Drug-tolerant persister cancer cells are vulnerable to GPX4 inhibition. Nature *551*, 247–250.

Harper, J.W., and Bennett, E.J. (2016). Proteome complexity and the forces that drive proteome imbalance. Nature *537*, 328–338.

Harrigan, J.A., Jacq, X., Martin, N.M., and Jackson, S.P. (2018). Deubiquitylating enzymes and drug discovery: emerging opportunities. Nat. Rev. Drug Discov. *17*, 57–78.

Harris, I.S., and Brugge, J.S. (2015). Cancer: the enemy of my enemy is my friend. Nature *527*, 170–171.

Harris, I.S., Treloar, A.E., Inoue, S., Sasaki, M., Gorrini, C., Lee, K.C., Yung, K.Y., Brenner, D., Knobbe-Thomsen, C.B., Cox, M.A., et al. (2015). Glutathione and thioredoxin antioxidant pathways synergize to drive cancer initiation and progression. Cancer Cell *27*, 211–222.

Hetz, C., Chevet, E., and Oakes, S.A. (2015). Proteostasis control by the unfolded protein response. Nat. Cell Biol. *17*, 829–838.

Hiramatsu, N., Messah, C., Han, J., LaVail, M.M., Kaufman, R.J., and Lin, J.H. (2014). Translational and posttranslational regulation of XIAP by eIF2alpha and ATF4 promotes ER stress-induced cell death during the unfolded protein response. Mol. Biol. Cell *25*, 1411–1420.

Hirono, I. (1961). Mechanism of natural and acquired resistance to methyl-bis-(beta-chlorethyl)-amine N-oxide in ascites tumors. Gan *52*, 39–48.

Hoadley, K.A., Yau, C., Hinoue, T., Wolf, D.M., Lazar, A.J., Drill, E., Shen, R., Taylor, A.M., Cherniack, A.D., Thorsson, V., et al. (2018). Cell-of-origin patterns dominate the molecular classification of 10,000 tumors from 33 types of cancer. Cell *173*, 291–304.e6.

Hong, A.L., Tseng, Y.-Y., Cowley, G.S., Jonas, O., Cheah, J.H., Kynnap, B.D., Doshi, M.B., Oh, C., Meyer, S.C., Church, A.J., et al. (2016). Integrated genetic and pharmacologic interrogation of rare cancers. Nat. Commun. *7*, 11987.

Huang, C.S., Anderson, M.E., and Meister, A. (1993). Amino acid sequence and function of the light subunit of rat kidney gamma-glutamylcysteine synthetase. J. Biol. Chem. *268*, 20578–20583.

Hwang, C., Sinskey, A.J., and Lodish, H.F. (1992). Oxidized redox state of glutathione in the endoplasmic reticulum. Science *257*, 1496–1502.

Jiang, L., Shestov, A.A., Swain, P., Yang, C., Parker, S.J., Wang, Q.A., Terada, L.S., Adams, N.D., McCabe, M.T., Pietrak, B., et al. (2016). Reductive carboxylation supports redox homeostasis during anchorage-independent growth. Nature *532*, 255–258.

Kim, Y.C., and Guan, K.-L. (2015). mTOR: a pharmacologic target for autophagy regulation. J. Clin. Invest. *125*, 25–32.

Klein, E.A., Thompson, I.M., Jr., Tangen, C.M., Crowley, J.J., Lucia, M.S., Goodman, P.J., Minasian, L.M., Ford, L.G., Parnes, H.L., Gaziano, J.M., et al. (2011). Vitamin E and the risk of prostate cancer: the selenium and vitamin E cancer prevention trial (SELECT). JAMA *306*, 1549–1556.

Komander, D., Clague, M.J., and Urbé, S. (2009). Breaking the chains: structure and function of the deubiquitinases. Nat. Rev. Mol. Cell Biol. *10*, 550–563.

Lauinger, L., Li, J., Shostak, A., Cemel, I.A., Ha, N., Zhang, Y., Merkl, P.E., Obermeyer, S., Stankovic-Valentin, N., Schafmeier, T., et al. (2017). Thiolutin is a zinc chelator that inhibits the Rpn11 and other JAMM metalloproteases. Nat. Chem. Biol. *13*, 709–714.

Le Gal, K., Ibrahim, M.X., Wiel, C., Sayin, V.I., Akula, M.K., Karlsson, C., Dalin, M.G., Akyürek, L.M., Lindahl, P., Nilsson, J., et al. (2015). Antioxidants can increase melanoma metastasis in mice. Sci. Transl. Med. *7*, re308.

Lee, J.-G., Baek, K., Soetandyo, N., and Ye, Y. (2013). Reversible inactivation of deubiquitinases by reactive oxygen species in vitro and in cells. Nat. Commun. *4*, 1568.

Lewerenz, J., Hewett, S.J., Huang, Y., Lambros, M., Gout, P.W., Kalivas, P.W., Massie, A., Smolders, I., Methner, A., Pergande, M., et al. (2013). The cystine/glutamate antiporter system x(c)(-) in health and disease: from molecular mechanisms to novel therapeutic opportunities. Antioxid. Redox Signal. *18*, 522–555.

Li, W., Xu, H., Xiao, T., Cong, L., Love, M.I., Zhang, F., Irizarry, R.A., Liu, J.S., Brown, M., and Liu, X.S. (2014). MAGeCK enables robust identification of essential genes from genome-scale CRISPR/Cas9 knockout screens. Genome Biol. *15*, 554.

Li, J., Yakushi, T., Parlati, F., Mackinnon, A.L., Perez, C., Ma, Y., Carter, K.P., Colayco, S., Magnuson, G., Brown, B., et al. (2017). Capzimin is a potent and specific inhibitor of proteasome isopeptidase Rpn11. Nat. Chem. Biol. *13*, 486–493.

Liu, Q., Xu, C., Kirubakaran, S., Zhang, X., Hur, W., Liu, Y., Kwiatkowski, N.P., Wang, J., Westover, K.D., Gao, P., et al. (2013). Characterization of Torin2, an ATP-competitive inhibitor of mTOR, ATM, and ATR. Cancer Res. *73*, 2574–2586.

Luo, J., Solimini, N.L., and Elledge, S.J. (2009). Principles of cancer therapy: oncogene and non-oncogene addiction. Cell *136*, 823–837.

Ma, X.M., and Blenis, J. (2009). Molecular mechanisms of mTOR-mediated translational control. Nat. Rev. Mol. Cell Biol. *10*, 307–318.

Maddocks, O.D., Berkers, C.R., Mason, S.M., Zheng, L., Blyth, K., Gottlieb, E., and Vousden, K.H. (2013). Serine starvation induces stress and p53-dependent metabolic remodelling in cancer cells. Nature *493*, 542–546.

Mandal, P.K., Schneider, M., Kölle, P., Kuhlencordt, P., Förster, H., Beck, H., Bornkamm, G.W., and Conrad, M. (2010). Loss of thioredoxin reductase 1 renders tumors highly susceptible to pharmacologic glutathione deprivation. Cancer Res. *70*, 9505–9514.

Meister, A., and Anderson, M.E. (1983). Glutathione. Annu. Rev. Biochem. *52*, 711–760.

Melo, E.P., Lopes, C., Gollwitzer, P., Lortz, S., Lenzen, S., Mehmeti, I., Kaminski, C.F., Ron, D., and Avezov, E. (2017). TriPer, an optical probe tuned to the endoplasmic reticulum tracks changes in luminal H2O2. BMC Biol. *15*, 24.

Mevissen, T.E.T., and Komander, D. (2017). Mechanisms of deubiquitinase specificity and regulation. Annu. Rev. Biochem. *86*, 159–192.

Meyer, H., Bug, M., and Bremer, S. (2012). Emerging functions of the VCP/p97 AAA-ATPase in the ubiquitin system. Nat. Cell Biol. *14*, 117–123.

Meyers, R.M., Bryan, J.G., McFarland, J.M., Weir, B.A., Sizemore, A.E., Xu, H., Dharia, N.V., Montgomery, P.G., Cowley, G.S., Pantel, S., et al. (2017). Computational correction of copy number effect improves specificity of CRISPR-Cas9 essentiality screens in cancer cells. Nat. Genet. *49*, 1779–1784.

Morimoto, R.I. (2008). Proteotoxic stress and inducible chaperone networks in neurodegenerative disease and aging. Genes Dev. *22*, 1427–1438.

Najm, F.J., Strand, C., Donovan, K.F., Hegde, M., Sanson, K.R., Vaimberg, E.W., Sullender, M.E., Hartenian, E., Kalani, Z., Fusi, N., et al. (2018). Orthologous CRISPR-Cas9 enzymes for combinatorial genetic screens. Nat. Biotechnol. *36*, 179–189.

Nicholson, B., and Suresh Kumar, K.G. (2011). The multifaceted roles of USP7: new therapeutic opportunities. Cell Biochem. Biophys. *60*, 61–68.

Ozcan, U., Ozcan, L., Yilmaz, E., Düvel, K., Sahin, M., Manning, B.D., and Hotamisligil, G.S. (2008). Loss of the tuberous sclerosis complex tumor suppressors triggers the unfolded protein response to regulate insulin signaling and apoptosis. Mol. Cell *29*, 541–551.

Piskounova, E., Agathocleous, M., Murphy, M.M., Hu, Z., Huddlestun, S.E., Zhao, Z., Leitch, A.M., Johnson, T.M., DeBerardinis, R.J., and Morrison, S.J. (2015). Oxidative stress inhibits distant metastasis by human melanoma cells. Nature *527*, 186–191.

Poole, L.B. (2015). The basics of thiols and cysteines in redox biology and chemistry. Free Radic. Biol. Med. *80*, 148–157.

Prigge, J.R., Coppo, L., Martin, S.S., Ogata, F., Miller, C.G., Bruschwein, M.D., Orlicky, D.J., Shearn, C.T., Kundert, J.A., Lytchier, J., et al. (2017). Hepatocyte hyperproliferation upon liver-specific co-disruption of Thioredoxin-1, Thioredoxin Reductase-1, and glutathione reductase. Cell Rep. *19*, 2771–2781.

Ramadan, K., Bruderer, R., Spiga, F.M., Popp, O., Baur, T., Gotta, M., and Meyer, H.H. (2007). Cdc48/p97 promotes reformation of the nucleus by extracting the kinase Aurora B from chromatin. Nature *450*, 1258–1262.

Reczek, C.R., and Chandel, N.S. (2015). ROS-dependent signal transduction. Curr. Opin. Cell Biol. *33*, 8–13.

Ritorto, M.S., Ewan, R., Perez-Oliva, A.B., Knebel, A., Buhrlage, S.J., Wightman, M., Kelly, S.M., Wood, N.T., Virdee, S., Gray, N.S., et al. (2014). Screening of DUB activity and specificity by MALDI-TOF mass spectrometry. Nat Commun. *5*, 4763.

Sachs, N., de Ligt, J., Kopper, O., Gogola, E., Bounova, G., Weeber, F., Balgobind, A.V., Wind, K., Gracanin, A., Begthel, H., et al. (2018). A living biobank of breast cancer organoids captures disease heterogeneity. Cell *172*, 373–386.e10.

Sayin, V.I., Ibrahim, M.X., Larsson, E., Nilsson, J.A., Lindahl, P., and Bergo, M.O. (2014). Antioxidants accelerate lung cancer progression in mice. Sci. Transl. Med. *6*, 221ra215.

Schwickart, M., Huang, X., Lill, J.R., Liu, J., Ferrando, R., French, D.M., Maecker, H., O'Rourke, K., Bazan, F., Eastham-Anderson, J., et al. (2010). Deubiquitinase USP9X stabilizes MCL1 and promotes tumour cell survival. Nature *463*, 103–107.

Selfors, L.M., Stover, D.G., Harris, I.S., Brugge, J.S., and Coloff, J.L. (2017). Identification of cancer genes that are independent of dominant proliferation and lineage programs. Proc. Natl. Acad. Sci. U S A *114*, E11276–E11284.

Shi, Z.Z., Osei-Frimpong, J., Kala, G., Kala, S.V., Barrios, R.J., Habib, G.M., Lukin, D.J., Danney, C.M., Matzuk, M.M., and Lieberman, M.W. (2000). Glutathione synthesis is essential for mouse development but not for cell growth in culture. Proc. Natl. Acad. Sci. U S A *97*, 5101–5106.

Sowa, M.E., Bennett, E.J., Gygi, S.P., and Harper, J.W. (2009). Defining the human deubiquitinating enzyme interaction landscape. Cell *138*, 389–403.

Stafford, W.C., Peng, X., Olofsson, M.H., Zhang, X., Luci, D.K., Lu, L., Cheng, Q., Tresaugues, L., Dexheimer, T.S., Coussens, N.P., et al. (2018). Irreversible inhibition of cytosolic thioredoxin reductase 1 as a mechanistic basis for anticancer therapy. Sci. Transl. Med. *10*.

Sun, S.C. (2008). Deubiquitylation and regulation of the immune response. Nat. Rev. Immunol. *8*, 501–511.

Trachootham, D., Alexandre, J., and Huang, P. (2009). Targeting cancer cells by ROS-mediated mechanisms: a radical therapeutic approach? Nat. Rev. Drug Discov. *8*, 579–591.

van der Reest, J., Lilla, S., Zheng, L., Zanivan, S., and Gottlieb, E. (2018). Proteome-wide analysis of cysteine oxidation reveals metabolic sensitivity to redox stress. Nat. Commun. *9*, 1581.

Villablanca, J.G., Volchenboum, S.L., Cho, H., Kang, M.H., Cohn, S.L., Anderson, C.P., Marachelian, A., Groshen, S., Tsao-Wei, D., Matthay, K.K., et al. (2016). A phase I new approaches to neuroblastoma therapy study of buthionine sulfoximine and melphalan with autologous stem cells for recurrent/refractory high-risk neuroblastoma. Pediatr. Blood Cancer *63*, 1349–1356.

Viswanathan, V.S., Ryan, M.J., Dhruv, H.D., Gill, S., Eichhoff, O.M., Seashore-Ludlow, B., Kaffenberger, S.D., Eaton, J.K., Shimada, K., Aguirre, A.J., et al. (2017). Dependency of a therapy-resistant state of cancer cells on a lipid peroxidase pathway. Nature *547*, 453–457.

Vora, S.R., Juric, D., Kim, N., Mino-Kenudson, M., Huynh, T., Costa, C., Lockerman, E.L., Pollack, S.F., Liu, M., Li, X., et al. (2014). CDK 4/6 inhibitors sensitize PIK3CA mutant breast cancer to PI3K inhibitors. Cancer Cell *26*, 136–149.

Wakil, S.J., and Abu-Elheiga, L.A. (2009). Fatty acid metabolism: target for metabolic syndrome. J. Lipid Res. *50*, S138–S143.

Wang, H., Nicolay, B.N., Chick, J.M., Gao, X., Geng, Y., Ren, H., Gao, H., Yang, G., Williams, J.A., Suski, J.M., et al. (2017). The metabolic function of cyclin D3–CDK6 kinase in cancer cell survival. Nature *546*, 426–430.

Wang, M., and Kaufman, R.J. (2014). The impact of the endoplasmic reticulum protein-folding environment on cancer development. Nat. Rev. Cancer *14*, 581–597.

Wang, Q., Li, L., and Ye, Y. (2008). Inhibition of p97-dependent protein degradation by Eeyarestatin I. J. Biol. Chem. *283*, 7445–7454.

Watanabe, T., Sagisaka, H., Arakawa, S., Shibaya, Y., Watanabe, M., Igarashi, I., Tanaka, K., Totsuka, S., Takasaki, W., and Manabe, S. (2003). A novel model of continuous depletion of glutathione in mice treated with L-buthionine (S,R)-sulfoximine. J. Toxicol. Sci. *28*, 455–469.

Whitesell, L., and Lindquist, S.L. (2005). HSP90 and the chaperoning of cancer. Nat. Rev. Cancer *5*, 761–772.

Winterbourn, C.C., and Hampton, M.B. (2008). Thiol chemistry and specificity in redox signaling. Free Radic. Biol. Med. *45*, 549–561.

Wu, K.C., Cui, J.Y., and Klaassen, C.D. (2011). Beneficial role of Nrf2 in regulating NADPH generation and consumption. Toxicol. Sci. *123*, 590–600.

Yang, W.S., SriRamaratnam, R., Welsch, M.E., Shimada, K., Skouta, R., Viswanathan, V.S., Cheah, J.H., Clemons, P.A., Shamji, A.F., Clish, C.B., et al. (2014). Regulation of ferroptotic cancer cell death by GPX4. Cell *156*, 317–331.

Zhang, J.H., Chung, T.D., and Oldenburg, K.R. (1999). A simple statistical parameter for use in evaluation and validation of high throughput screening assays. J. Biomol. Screen. *4*, 67–73.

Please cite this article in press as: Harris et al., Deubiquitinases Maintain Protein Homeostasis and Survival of Cancer Cells upon Glutathione Depletion, Cell Metabolism (2019), https://doi.org/10.1016/j.cmet.2019.01.020

STAR★METHODS

KEY RESOURCES TABLE

REAGENT or RESOURCE	SOURCE	IDENTIFIER
Antibodies		
Mouse monoclonal antibody anti-GCLC (γ-GCSc; H-5)	Santa Cruz	Cat# sc-390811; RRID: AB_2736837
Rabbit polyclonal antibody anti-USP7	Bethyl Laboratories	Cat# A300-033A; RRID: AB_203276
Mouse monoclonal antibody anti-ubiquitin (P4D1)	BioLegend	Cat# 646302; RRID: AB_1659269
Rabbit monoclonal antibody anti-HMOX1 (HO-1; D60G11	Cell Signaling Technologies	Cat# 5853; RRID: AB_10835857
Mouse monoclonal antibody anti-HSP70 (W27)	BioLegend	Cat# 648002; RRID: AB_2264228
Rat monoclonal antibody anti-BiP (76-E6)	BioLegend	Cat# 644402; RRID: AB_2248519
Rabbit monoclonal antibody anti-ATF4 (D4B8)	Cell Signaling Technologies	Cat# 11815; RRID: AB_2616025
Mouse monoclonal antibody anti-HA (HA-7)	Abcam	Cat# ab49969; RRID: AB_880330
Rabbit monoclonal antibody anti-USP7 (HAUSP; D17C6)	Cell Signaling Technologies	Cat# 4833; RRID: AB_10557113
Mouse monoclonal anti-USP8 (UBPY; E-1)	Santa Cruz	Cat# sc-376130; RRID: AB_10991111
Rabbit monoclonal anti-USP10 (D7A5)	Cell Signaling Technologies	Cat# 8501S; RRID: AB_10949976
Rabbit polyclonal antibody anti-XIAP	Cell Signaling Technologies	Cat# 2042; RRID: AB_2214870
Rabbit polyclonal antibody anti-TRXR1	Cell Signaling Technologies	Cat# 6925; RRID: AB_10839114
Mouse monoclonal antibody anti-TrxR1	Santa Cruz	Cat# sc-28321; RRID: AB_628405
Rabbit monoclonal antibody anti-GPX4	Abcam	Cat# ab125066; RRID: AB_10973901
Rabbit monoclonal antibody anti-TXN1	Cell Signaling Technologies	Cat# 2429; RRID: AB_2272594
Mouse monoclonal antibody anti-beta-Actin	Sigma-Aldrich	Cat# A1978; RRID: AB_476692
Mouse monoclonal antibody anti-beta-Actin	Thermo Fisher	Cat# MA1-91399; RRID: AB_2273656
Chemicals, Peptides, and Recombinant Proteins		
L-Buthionine sulfoximine	Sigma-Aldrich	Cat# B2515
MI-2	Selleck Chemicals	Cat# S7429
PR-619	Selleck Chemicals	Cat# S7130
Eeyarestatin I (EERI)	Tocris	Cat# 3922
Sulfasalazine (SSA)	Sigma-Aldrich	Cat# S0883
N-Acetyl-L-cysteine (NAC)	Sigma-Aldrich	Cat# A7250
(±)-6-Hydroxy-2,5,7,8-tetramethylchromane-2-carboxylic acid (Trolox)	Sigma-Aldrich	Cat# 238813
Ferrostatin-1 (Fer1)	Sigma-Aldrich	Cat# SML0583
Glutathione reduced ethyl ester	Sigma-Aldrich	Cat# G1404
Aurothioglucose hydrate (ATG)	Sigma-Aldrich	Cat# A0606
Birinapant	Selleck Chemicals	Cat# S7015
Torin2	Selleck Chemicals	Cat# S2817
Tunicamycin	Tocris	Cat# 3516
HBX 19818	MedChemExpress	Cat# HY-17540
bisBenzimide H 33342 trihydrochloride (Hoechst)	Sigma-Aldrich	Cat# 14533
ExTaq DNA Polymerase	TaKaRa	Cat# RR001A
SuperSignal West Pico PLUS chemiluminescent substrate	Thermo Fisher	Cat# 34578
Annexin V, Alexa Fluor 488 conjugate	Thermo Fisher Scientific	Cat# A13201
Propidium iodide (PI)	Sigma-Aldrich	Cat# P4170
BODIPY 581/591 C11 (Lipid Peroxidation Sensor)	Thermo Fisher Scientific	Cat# D3861
Critical Commercial Assays		
QIAamp DNA Blood Midi Kit	Qiagen	Cat# 51183
GSH-Glo kit	Promega	Cat# V6911
PureLink RNA Mini Kit	Life Technologies	Cat# 12183025

(*Continued on next page*)

Continued

REAGENT or RESOURCE	SOURCE	IDENTIFIER
qScript cDNA Synthesis kit	QuantaBio	Cat# 95047-100
Thioredoxin Reductase 1 (TXNRD1) Activity Assay Kit	Abcam	Cat# ab190804
Experimental Models: Cell Lines		
OAW28	Laboratory of Dennis Slamon	N/A
TYK-NU	Laboratory of Dennis Slamon	N/A
NCI-H1568	ATCC	Cat# CRL-5876; RRID: CVCL_1476
HCC1937	ATCC	Cat# CRL-2336; RRID: CVCL_0290
EFM-19	Laboratory of Dennis Slamon	N/A
NCI-H522	ATCC	Cat# CRL-5810; RRID: CVCL_1567
BT-20	ATCC	Cat# HTB-19; RRID: CVCL_0178
BT-549	ATCC	Cat# HTB-122; RRID: CVCL_1092
HCC1143	ATCC	Cat# CRL-2321; RRID: CVCL_1245
HCC1569	ATCC	Cat# CRL-2330; RRID: CVCL_1255
HCC1806	ATCC	Cat# CRL-2335; RRID: CVCL_1258
HCC1954	ATCC	Cat# CRL-2338; RRID: CVCL_1259
HCC38	ATCC	Cat# CRL-2314; RRID: CVCL_1267
HCC70	ATCC	Cat# CRL-2315; RRID: CVCL_1270
MDA-MB-231	ATCC	Cat# HTB-26; RRID: CVCL_0062
MDA-MB-436	ATCC	Cat# HTB-130; RRID: CVCL_0623
MDA-MB-468	ATCC	Cat# HTB-132; RRID: CVCL_0419
BT-474	ATCC	Cat# HTB-20; RRID: CVCL_0179
EFM-192A	Laboratory of Dennis Slamon	N/A
HCC1419	ATCC	Cat# CRL-2326; RRID: CVCL_1251
HCC1500	ATCC	Cat# CRL-2329; RRID: CVCL_1254
HCC202	ATCC	Cat# CRL-2316; RRID: CVCL_2062
MCF-7	ATCC	Cat# HTB-22; RRID: CVCL_0031
MDA-MB-175-VII	ATCC	Cat# HTB-25; RRID: CVCL_1400
MDA-MB-361	ATCC	Cat# HTB-27; RRID: CVCL_0620
SKBR3	ATCC	Cat# HTB-30; RRID: CVCL_0033
T-47D	ATCC	Cat# HTB-133; RRID: CVCL_0553
UACC-812	ATCC	Cat# CRL-1897; RRID: CVCL_1781
ZR-75-1	ATCC	Cat# CRL-1500; RRID: CVCL_0588
ZR-75-30	ATCC	Cat# CRL-1504; RRID: CVCL_1661
A549	ATCC	Cat# CCL-185; RRID: CVCL_0023
NCI-H1299	ATCC	Cat# CRL-5803; RRID: CVCL_0060
NCI-H1437	ATCC	Cat# CRL-5872; RRID: CVCL_1472
NCI-H1838	ATCC	Cat# CRL-5899; RRID: CVCL_1499
NCI-H1975	ATCC	Cat# CRL-5908; RRID: CVCL_1511
NCI-H2030	ATCC	Cat# CRL-5914; RRID: CVCL_1517
NCI-H2122	ATCC	Cat# CRL-5985; RRID: CVCL_1531
NCI-H2228	ATCC	Cat# CRL-5935; RRID: CVCL_1543
NCI-H358	ATCC	Cat# CRL-5807; RRID: CVCL_1559
NCI-H460	ATCC	Cat# HTB-177; RRID: CVCL_0459
Caov-3	ATCC	Cat# HTB-75; RRID: CVCL_0201
JHOM-1	Laboratory of Dennis Slamon	N/A
KURAMOCHI	Laboratory of Dennis Slamon	N/A
OVCAR-5	Laboratory of Dennis Slamon	N/A
OVCAR-8	Laboratory of Dennis Slamon	N/A
OV-90	ATCC	Cat# CRL-11732; RRID: CVCL_3768

(*Continued on next page*)

Continued

REAGENT or RESOURCE	SOURCE	IDENTIFIER
OVSAHO	Laboratory of Dennis Slamon	N/A
RMUGS	Laboratory of Dennis Slamon	N/A
Oligonucleotides		
Primers used for the construction of sgRNA guides: listed in Table S6	This paper	N/A
Primers used quantitative PCR: listed in Table S6	This paper	N/A
Recombinant DNA		
LentiCrispr v2	Addgene	Cat# 52961
psPAX2	Addgene	Cat# 12260
pMD2.G	Addgene	Cat# 12259
Software and Algorithms		
GraphPad Prism 7.0	GraphPad Prism Software	N/A

CONTACT FOR REAGENT AND RESOURCE SHARING

Further information and requests for reagents may be directed to and will be fulfilled by the Lead Contact, Joan S. Brugge (joan_brugge@hms.harvard.edu).

EXPERIMENTAL MODEL AND SUBJECT DETAILS

Animal Studies

All animal studies were performed according to protocols approved by the Institutional Animal Care and Use Committee, the Standing Committee on Animals at Harvard University. Two million HCC-1806 breast cancer cells were subcutaneously injected into the right flank of 6-7 week old female nude mice (NU/J; Jackson Laboratory #002019). Tumor volume was determined using caliper measurements and the oblate ellipsoid volume formula ($V = \pi/6*a*b$, where a and b represent the shortest and longest diameters, respectively). Once tumors reached ~300 mm3, mice were randomized into six treatment arms: (1) vehicle + water; (2) vehicle + BSO; (3) MI-2 (10mg/kg) + water; (4) MI-2 (10mg/kg) + BSO; (5) MI-2 (20mg/kg) + water; and (6) MI-2 (20mg/kg) + BSO. Vehicle for MI-2 was 5% DMSO, 45% PEG400 and 50% phosphate-free saline. MI-2 and BSO were formulated and delivered as previously described (Fontan et al., 2012; Watanabe et al., 2003).

Cell Culture

All cell lines were maintained in RPMI (Thermo Fisher #11875119) with 10% fetal bovine serum (FBS; Sigma #12306C) and 1% penicillin and streptomycin (Thermo Fisher #15070063). Cell lines used were obtained from ATCC or through a collaboration with the lab of Dr. Dennis Slamon. NCI-H1568, HCC1937, NCI-H522, BT-20, BT-549, HCC1143, HCC1569, HCC1806, HCC1954, HCC38, HCC70, MDA-MB-231, MDA-MB-436, MDA-MB-468, BT-474, HCC1419, HCC1500, HCC202, MCF-7, MDA-MB-175-VII, MDA-MB-361, SKBR3, T-47D, UACC-812, ZR-75-1, ZR-75-30, A549, NCI-H1299, NCI-H1437, NCI-H1838, NCI-H1975, NCI-H2030, NCI-H2122, NCI-H2228, NCI-H358, NCI-H460, Caov-3, OV-90 were provided by ATCC and OAW28, TYK-NU, EFM-19, EFM-192A, JHOM-1, KURAMOCHI, OVCAR-5, OVCAR-8 OVSAHO, RMUGS were provided by the laboratory of Dennis Slamon. All cell lines were authenticated and negative for mycoplasma contamination.

METHOD DETAILS

Quantification of Cell Numbers

For high-throughput experiments in 96-well (BD Biosciences #353219) or 384-well (Corning #3764) plate formats, cells were washed with PBS (Corning #21-031-CV), fixed using 4% formaldehyde (Sigma #252549) and stained with 5 μg/ml bisBenzimide H 33342 trihydrochloride (Hoechst; Sigma #14533). Cell numbers were determined by imaging plates and quantifying nuclei using the Acumen Cellista plate cytometer (TTP Labtech). Data post-processing was conducted using R and Prism scripts. For all other experiments in 6-well plate format, cells were washed with PBS, detached using 0.25% trypsin (Corning #25053CI) and counted using a Beckman Coulter particle counter.

Compound Library

To generate a focused compound library, compounds were purchased from Selleck Chemicals, Tocris and Sigma, either dissolved in dimethyl sulfoxide (DMSO, 472301 Sigma) at 10 mM or as dry powder that was dissolved at 10 mM in DMSO. Experimental compounds were excluded from the outer two rows and columns of each 384-well library plate to avoid the potential impact of edge

effects. Each compound screen plate contained 24 compounds arrayed across a 10-point dose curve ranging from 20 μM to 3 nM (24 compound plates in total). To generate library plates, 75 μL of compound were pipetted into the wells of column 3 (C3-N3) and 13 (C13-N13) of an AB0781 plate (Thermo Fisher Scientific). Using an Agilent Bravo, 50 μl of DMSO were pipetted into the remaining wells. Three-fold serial dilutions were then created by aspirating 25 μl of compound (starting in columns 3 and 13) and dispensing into 50 μl of DMSO in the adjacent column, pipetting up and down five times and then transferring 25 μL to the next column. The resultant master compound plates contained at least 50 μl of compound at the desired range of concentrations (10 mM to 0.5 μM; corresponding to 20 μM to 3 nM final concentration in cells). Library screening plates were created by aspirating 11 μL of compound from the AB0781 master plates to AB1056 plates (Thermo Fisher Scientific).

High-Throughput Compound Screening

For screening in 384-well plates, a seeding density of 300 cells per well for HCC-1806 and 750 cells per well for MDA-MB-468 breast cancer cell lines was chosen. Assay robustness was determined by obtaining a Z' factor (Zhang et al., 1999) for each cell line. Cells were treated with DMSO or the cytotoxic agent vincristine (1 μM) or taxol (1 μM) for 72 h and average (AVG) and standard deviation (SD) of the number of cells was used to determine the Z' factor ($Z' = 1 - ((3SD_{DMSO}+3SD_{Cytotoxic})/(AVG_{DMSO}-AVG_{Cytotoxic}))$. The Z' factor was determined to be 0.55 for HCC-1806 and 0.75 for MDA-MB-468 breast cancer cell lines. To determine compounds that sensitize cells to inhibition of GCLC, cells were seeded in 30 μl at their respective cell densities. After 24 h, 20 μl media containing vehicle or 100 μM BSO was added. After 24 h, compounds from the library plates were pin-transferred (100 nl) onto the cells. After 72 h, cells were washed with PBS (Thermo Fisher), fixed using 4% formaldehyde (Sigma #252549) and stained with 5 μg/ml bisBenzimide H 33342 trihydrochloride (Hoechst; Sigma #14533). Cell numbers were determined by imaging plates and quantifying nuclei using the Acumen Cellista plate cytometer (TTP Labtech). Data post-processing was conducted using R and Prism scripts.

CRISPR-Cas9 screening

Druggable Cancer Targets v2.1 is a second generation CRISPR-Cas9 library based upon prior studies (Hong et al., 2016). 5,566 sgRNAs targeting 798 genes were generated using the "Rule Set 2" method as previously described (Doench et al., 2016). In addition, 300 non-targeting sgRNA controls were included for a total of 5,866 sgRNA in this pooled library. Oligos to generate the sgRNAs (Table S2) were synthesized by CustomArray (Bothell, WA). The oligos were introduced into pXPR_BRD050 and the subsequent sgRNAs were sequenced verified. Lentivirus was generated by the Broad Institute's Genetic Perturbation Platform at a viral titer (based on the A549 cell line) of 1.82e7 viral particles/mL. HCC-1806 breast cancer cells were infected with virus containing plenti-EF1-IRES-Cas9-Neo construct and selected with 1 mg/ml G418. Cas9 activity was determined to be 79.6% in HCC-1806 cells by infecting cells with virus containing GFP-Cas9-sgGFP-Puro construct (pXPR_011v2), selecting with 2 μg/ml puromycin. Next, the amount of virus required for a MOI of 0.3 was determined to be 18.4 μl virus for 1.5 million HCC-1806 cells by infecting cells with a range of virus amounts and selecting with 2 μg/ml puromycin and counting viable cells once the uninfected cells had completely died. The representation of the library in the screen was maintained at 2000 fold throughout the experiment (~12 million cells per condition). Cell pellets were harvested for gDNA using QIAamp DNA Blood Midi Kit (Qiagen #51183), the barcode region was amplified using ExTaq DNA Polymerase (TaKaRa #RR001A) and next-gene sequencing was conducted using HiSeq 2500 (Illumina). Barcode representation was determined using MAGeCK analysis (Li et al., 2014).

Quantification of Cell Death

For quantification of cell death, cells were plated in 6-well plates and treated with indicated compounds. At the endpoint, supernatant was collected and cells were washed with PBS and this was also collected. Trypsin was added to detached cells and then inactivated with the addition of media containing 10% FBS. Collected cells were washed and resuspended with Annexin V buffer (10 mM HEPES, 150 mM NaCl, 2.5 mM $CaCl_2$, pH = 7.4) containing Annexin V Alexa Fluor 488 conjugate (Thermo Fisher #A13201) and propidium iodide (Sigma # P4170). Annexin V positive cells were determined using FACSCalibur (BD Biosciences) and FlowJo software.

GSH Determination

Cells were seeded into 96-well white plates (Corning #3917) and treated with BSO or DUB inhibitors (MI-2, PR-619, EERI) for indicated time points. Cells were washed with PBS and GSH levels were determined using GSH-Glo kit (Promega #V6911).

Immunoblot analysis

Cells were lyzed in RIPA buffer (Boston BioProducts #BP-115) containing phosphatase inhibitor cocktail (100X; Bimake #B15002), protease inhibitor cocktail (100X; Bimake #B14002) and proteasome inhibitor (10 μM MG-132; Sigma #M7449). Protein quantification was conducted using Pierce BCA protein assay kit (Thermo Fisher #23225). Protein lysates were treated Laemmli SDS sample buffer (6X; Boston BioProducts # BP-111R) with 5% β-mercaptoethanol for 10 min at 95°C. Samples were run on 4-20% Criterion TGX precast gels (Bio-Rad #5671093), transferred onto Immobilon-PSQ PVDF membranes (MilliporeSigma #ISEQ00010). Membranes were blocked with %5 milk in TBST for 1 hour and stained overnight with indicated antibodies in %5 milk with TBST. Antibody signal was visualized using SuperSignal West Pico PLUS chemiluminescent substrate (Thermo Fisher #34578) and HyBlot CL film (Denville

Scientific #E3018). The following antibodies were used for immunoblot analysis: mouse monoclonal antibodies anti-GCLC (γ-GCSc; H-5) (RRID: AB_2736837), anti-ubiquitin (P4D1) (RRID: AB_1659269), anti-HSP70 (W27) (RRID: AB_2264228), anti-HA (HA-7) (RRID: AB_880330), anti-TrxR1 (RRID: AB_628405), anti-beta-Actin (RRID: AB_476692); rabbit polyclonal antibodies anti-USP7 (RRID: AB_203276), anti-XIAP (RRID: AB_2214870), anti-TRXR1 (RRID: AB_10839114); rabbit monoclonal antibodies anti-HMOX1 (HO-1; D60G11) (RRID: AB_10835857), anti-ATF4 (D4B8) (RRID: AB_2616025), anti-GPX4 (RRID: AB_10973901); rat monoclonal antibody anti-BiP (76-E6) (RRID: AB_2248519).

sgRNAs Cloning, Virus Production and Infection of Cells

Using BsmBI restriction sites, primers (Table S6) were annealed and cloned into LentiCrispr v2. HEK293T cells were transfected with LentiCrispr v2 sgRNA vectors and packaging plasmids psPAX2 (Addgene #12260) and pMD2.G (Addgene #12259) using polyethylenimine (PEI) and Opti-MEM (Thermo Fisher # 31985062). After 24-72 hours, supernatant was harvested, filtered using a Puradisc 25 mm / 0.45 μm filter (Whatman #6780-2504) and added to HCC-1806 cells along with 8 μg/ml polybrene (hexadimethrine bromide; Sigma # H9268). After 24 hours, virus was removed and replaced with fresh RPMI media with 10% FBS. After 24 hours, media containing puromycin (2 μg/ml) was added to select for infected cells. Once non-infected cells with media containing puromycin were completely dead, cells were expanded and cultured without puromycin.

Quantitative RT-PCR Analysis and Primers

mRNA was isolated from cells using PureLink RNA Mini Kit (Life Technologies #12183025) and cDNA was synthesized using qScript cDNA Synthesis kit (QuantaBio #95047-100). Quantitative real-time (RT) PCR was conducted using QuantStudio 7 Flex Real-Time PCR System (Thermo Fisher) with Power SYBR Green PCR Mix (Thermo Fisher) and primers against target genes (Table S6).

DUB Target Engagement Using HA-Ub-VS Probe

HEK293T cells were seeded, allowed to adhere for 24 hours, then treated with MI-2 (Selleck Chemicals) or DUB inhibitor HBX 19818 (MedChemExpress #HY-17540) for 6 or 15 hours. Cells were harvested and lysed in lysis buffer (20 mM Tris pH 8.0 buffer with 1% NP-40, 150 mM NaCl, 10% glycerol, and 1x HALT protease inhibitor cocktail (ThermoFisher # 87786)). The lysate samples were diluted to 50 μg in 30 μL of lysate buffer, DTT was added to 1 mM, and the samples were incubated for 15 minutes at room temperature. The HA-ubiquitin-vinylmethylsulfone (HA-Ub-VS) probe (0.25 μg) was added and the samples were incubated for 30 minutes at room temperature on a rocker. The samples were then denatured by adding LDS buffer (10% BME) and heating for 5-10 minutes at 95°C. The samples (12 μg lysate) were analyzed by western blot using the following antibodies: HA (Abcam #ab49969) (RRID: AB_880330), USP7 (Cell Signaling Technologies #4833) (RRID: AB_10557113), USP8 (Santa Cruz #sc-376130) (RRID: AB_10991111), and USP10 (Cell Signaling Technologies #8501) (RRID: AB_10949976).

Development of Mammary Organoid Cultures

Human mammary tissues were obtained from elective reduction mammoplasties or prophylactic mastectomies, and were processed on the day of surgery. All samples are collected in accordance with protection of human subjects protocols. This study was deemed 'not human subjects research' by the Harvard Institutional Review Board. All patients were consented for tissue distribution. Normal mouse mammary glands were obtained from normal C57BL/6J murine #4 mammary glands. Human and mouse mammary samples were digested to the organoid level using collagenase for 1-2 hours, and embedded in a basement membrane extract droplet. This was overlaid with a fully defined organoid medium as described (Sachs et al., 2018). Cultures were passaged via enzymatic digestion with TrypLE and re-embedded in basement membrane extract, also as described (Sachs et al., 2018).

Determination of TXNRD1 Activity

TXNRD1 activity was determined using the TXNRD1 activity assay kit (Abcam # ab190804). Briefly, HCC-1806 breast cancer cell lysates (1 mg/ml) were incubated with DUB inhibitors MI-2, PR-619 and EERI or positive controls auranofin (AUR) and aurothioglucose (ATG) for 30 min. Samples were transferred to a plate coated with TXNRD1 antibody and incubated for 2 hours. The plate was subsequently washed three times, and TXNRD1-specific activity was measured after the addition of NADPH and DTNB in reaction buffer by measuring absorbance at 412 nm every minute for 60 minutes. The rate of increase in absorbance was calculated and used as TXNRD1 activity.

Detection of Redox State of Thioredoxin 1

800,000 cells were seeded on 10 cm dishes, followed by treatment with DMSO (0.1%), BSO (100 μM), Auranofin (250 nM), MI-2 (1 μM), PR-619 (5 μM), or EERI (2 μM) for 24 hours, or Auranofin (5 μM) for 4 hours. Cells were washed in PBS and lysed in 150 μL urea lysis buffer containing IAM as previously described (Du et al., 2013) to alkylate free thiols, followed by reduction and alkylation of disulfides with IAA. For the fully reduced or oxidized control samples, cell lysates were treated with DTT followed by IAA or IAM. Protein extracts were mixed with 4X non-reducing sample buffer (32% glycerol, 0.4% bromphenol blue in Urea lysis buffer). 40 μg of protein was separated by urea-PAGE (8M Urea, 9% acrylamide separating gel; 8M Urea, 4% acrylamide stacking gel),

followed by transfer to 0.45m Nitrocellulose membranes (GE Healthcare). For total protein analysis, 20 μg of protein were mixed with 6X reducing sample buffer containing beta-ME and separated by SDS-PAGE using NuPAGE 4-12% Bis-Tris gels (Invitrogen), followed by transfer to 0.45 μm Nitrocellulose membranes. The membranes were blocked in 5% non-fat milk in TBST, followed by immunoblotting. The following antibodies were used: TXN1 (Cell Signaling Technologies, Cat# 2429S, Lot# 3) (RRID: AB_2272594) and beta-actin (Thermo Fisher, clone AC-15) (RRID: AB_2273656).

QUANTIFICATION AND STATISTICAL ANALYSIS

Image and Statistical Analysis

Quantification of band intensity for immunoblots were determined using ImageJ. Differential expression analysis of RNA-seq from CCLE was conducted using R. All other statistical analysis was completed using Prism.